The long-non coding RNA HOTAIR as site specific regulator of inflammation in chronic arthritis

Muriel elhai
UniversitätsSpital Zürich Zentrum für Experimentelle Rheumatologie https://orcid.org/0000-0001-8627-5758

Raphael Micheroli
University Hospital Zurich

Miranda Houtman
University Hospital Zurich

Masoumeh Mirrahimi
Center of Experimental Rheumatology, Department of Rheumatology, University Hospital of Zurich, University of Zurich

Larissa Moser
Center of Experimental Rheumatology, Department of Rheumatology, University Hospital of Zurich, University of Zurich

Chantal Pauli
University Hospital Zürich and the University of Zurich

Kristina Bürki
Center of Experimental Rheumatology, Department of Rheumatology, University Hospital of Zurich, University of Zurich

Andrea Laimbacher
Center of Experimental Rheumatology, Department of Rheumatology, University Hospital of Zurich, University of Zurich

Gabriela Kania
Center of Experimental Rheumatology, Department of Rheumatology, University Hospital Zürich

Kerstin Klein
Department of Rheumatology and Immunology, University Hospital Bern

Philipp Schätzle
Cytometry Facility, University of Zurich

Mojca Frank Bertoncelj
Center of Experimental Rheumatology, Department of Rheumatology, University Hospital of Zurich, University of Zurich

Sam Edalat
University Hospital Zurich

Maria Sakkou

Biomedical Sciences Research Center Alexander Fleming

George Kollias

B.S.R.C. Alexander Fleming https://orcid.org/0000-0003-1867-3150

Marietta Armaka

Biomedical Sciences Research Center Alexander Fleming https://orcid.org/0000-0003-0985-9076

Oliver Distler

Center of Experimental Rheumatology, Department of Rheumatology, University Hospital Zürich

Caroline Ospelt (caroline.ospelt@usz.ch)

Department of Rheumatology, Center of Experimental Rheumatology, University Hospital Zurich, University of Zurich https://orcid.org/0000-0002-9151-4650

Article

Keywords: HOTAIR, synovial fibroblast, epigenetic, arthritis

Posted Date: February 10th, 2023

DOI: https://doi.org/10.21203/rs.3.rs-2543547/v1

Additional Declarations: There is **NO** Competing Interest.

Version of Record: A version of this preprint was published at Nature Communications on December 9th, 2023. See the published version at https://doi.org/10.1038/s41467-023-44053-w.

The long-non coding RNA *HOTAIR* as site specific regulator of inflammation in chronic arthritis

Muriel Elhai[1], Raphael Micheroli[1], Miranda Houtman[1], Masoumeh Mirrahimi[1], Larissa Moser[1], Chantal Pauli[2], Kristina Bürki[1] , Andrea Laimbacher[1], Gabriela Kania[1], Kerstin Klein[1,3,4], Philipp Schätzle[5], Mojca Frank Bertoncelj[1], Sam G. Edalat[1], Maria Sakkou[6,7], George Kollias[6,7], Marietta Armaka[8], Oliver Distler[1], Caroline Ospelt[1*]

[1]Center of Experimental Rheumatology, Department of Rheumatology, University Hospital of Zurich, University of Zurich, Zurich, Switzerland

[2]Institute for Pathology and Molecular Pathology, University Hospital Zurich, Zurich 8091, Switzerland

[3]Department of BioMedical Research, University of Bern, Bern, Switzerland

[4]Department of Rheumatology and Immunology, University Hospital Bern, Bern, Switzerland

[5]Cytometry Facility, University of Zurich, Zurich Switzerland

[6]Institute for Bioinnovation, Biomedical Sciences Research Center (BSRC) 'Alexander Fleming', Vari, Greece

[7]Department of Physiology, Medical School, National and Kapodistrian University of Athens, Athens, Greece

[8]Institute for Fundamental Biomedical Research, Biomedical Sciences Research Center "Alexander Fleming", Vari, Greece.

CORRESPONDING AUTHOR

Caroline Ospelt,

Center of Experimental Rheumatology, Departement of Rheumatology, University Hospital of Zurich, University of Zurich, Rämistrasse 100, CH-8091, Zurich, Switzerland

caroline.ospelt@usz.ch

ABSTRACT

Most forms of arthritis, have a distinctive topographical pattern of joint involvement. Beyond these differences among diseases, there are also differences in phenotype and response to treatment between joints of the same type of arthritis, suggesting that molecular mechanisms may differ depending on joint location. Here we show that there are joint-specific molecular and tissue changes in the synovium and in local stromal cells (synovial fibroblasts;SF). The long non-coding RNA *HOTAIR*, expressed only in lower extremities SF, regulates much of this site-specific gene expression in SF. Downregulation of *HOTAIR* after TNF stimulation regulated relevant inflammatory pathways by epigenetic and transcriptional mechanisms and modified the migratory function of SF, decreased SF-mediated osteoclastogenesis, and increased the attraction of B cells by SF. Since site-specific expression of *HOTAIR* was also measured in the skin, spine and gastrointestinal tract, we propose *HOTAIR* as important epigenetic factor that modulates site-specific phenotypes of chronic inflammation.

TEASER

HOTAIR as important epigenetic factor that modulates site-specific phenotypes of chronic inflammation.

Keywords: HOTAIR, synovial fibroblast, epigenetic, arthritis

80 **GRAPHICAL ABSTRACT**

81 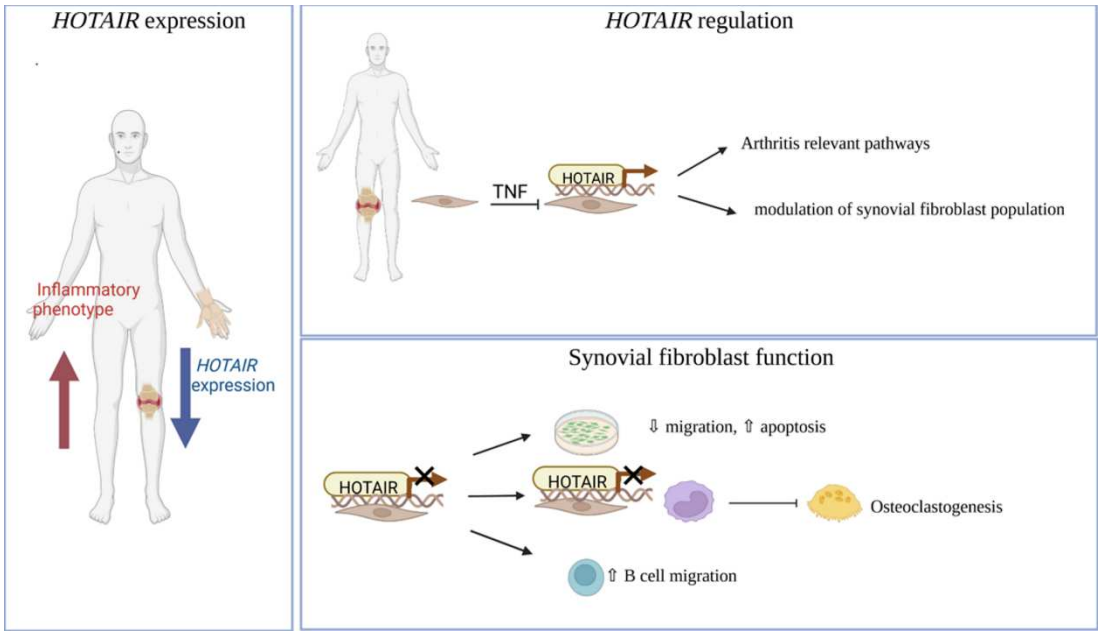

82

83

84

85

86

87

88

89

90

91

92

93

94

95

96

INTRODUCTION

Chronic arthritis is a major public health problem, which has a substantial influence on health and quality of life(*1*). Most forms of arthritis, including rheumatoid arthritis (RA), osteoarthritis (OA) and spondyloarthritis, have a distinctive topographical pattern of joint involvement(*2*). Among them, RA is the most frequent autoimmune arthritis, affecting 1% of the population(*3*). Despite the advances made in the management of RA in the last decades, 6 - 17% of the patients remain refractory to immunosuppressive treatment(*4*).

Although patients with untreated RA typically exhibit a symmetrical polyarthritis, individuals with refractory disease might develop a less extensive pattern of polyarthritis, an oligoarticular or even a monoarticular disease, suggesting that immunosuppressive therapy might be effective in some joints and not in others(*5*). Thus, beyond differences between diseases, there are also differences in phenotype and response to treatment depending on the joints within the same type of arthritis, suggesting that molecular mechanisms may differ according to joint location.

Deciphering the heterogeneity of synovium at both the cellular and molecular levels has revolutionized the understanding of the pathogene(*6-9*). In particular, refractory RA has been associated with a pauci-immune, fibroid pathotype of the synovium and a molecular signature suggestive of activated fibroblasts(*10*). Activation of synovial fibroblasts (SF) has long been known to play a critical role in joint inflammation and destruction(*11, 12*), but has attracted considerable attention more recently due to the discovery of pathogenic subpopulations of SF in the synovium through single-cell analysis(*10, 13-16*). Changes in the epigenetic landscape have been shown to be central to the permanent activation and aggressiveness of SF in RA(*12*).

121 We have previously demonstrated the existence of transcriptomic, epigenetic and
122 functional changes of SF depending on their joint location(*17*). This specific stromal
123 signature in particular concerned genes involved in the embryonic development of the
124 respective joint regions (i.e. *HOX* genes), suggesting an embryonically imprinted joint
125 specific stromal signature. In particular, the HOX transcript antisense intergenic RNA
126 (HOTAIR), which is an important regulator of the epigenetic landscape(*18*), was
127 exclusively expressed in joints of the lower extremity in human and in mice(*17*).
128 *HOX* genes encode a family of transcriptional regulators, which are involved in
129 distinct developmental programmes along the head-tail axis of vertebrates(*19*).
130 Moreover, they remain site-specifically expressed in several differentiated tissues, e.g.
131 in cartilage, the skin, the vasculature and gastrointestinal tract(*17, 18, 20-24*).
132 It remains to be determined whether differences between the phenotype of arthritis at
133 the tissue and molecular levels depend on its location, and if so whether the site-
134 specific expression of *HOX* genes is involved in these changes.
135 Here, we showed that there are joint-specific molecular and tissue changes in RA and
136 that the long non-coding RNA (lncRNA) *HOTAIR* (HOX transcript antisense RNA) is
137 a master regulator of joint-specific gene expression in arthritic SF. Down-regulation
138 of *HOTAIR* in an inflammatory environment led to activation of specific arthritis
139 relevant pathways and changes in SF function, that might modulate the arthritis
140 phenotype in lower extremity joints.
141

142 **RESULTS**

143 **Joint-specific histological and molecular differences in RA**

144 We first analysed joint-specific differences in the synovium of RA patients using a
145 multi-level approach including histological and molecular analysis. Comparison of the
146 histological grade of synovitis(*25*) between hand and knee RA showed a trend towards
147 a higher synovitis score in RA hands (mean: 5.25 ± 1.78) compared to RA knees
148 (mean: 4.31 ± 1.78; difference -0.94 ± 0.52, p=0.076), as previously seen(*17*) (Figure
149 1A). Accordingly, vascular density of the synovium was higher in RA hand synovium,
150 with a larger percentage of patients having highly vascularised synovium in the hands
151 than in the knees (54% vs. 37% p=0.031) (Figure 1B). Assessment of synovial
152 pathotypes as defined by Humby et al.(*9*) in hand and knee RA showed a
153 predominance of the lymphoid pathotype in hand RA, whereas the pathotypes were
154 balanced in the knees (Figure 1C). The lymphoid pathotype presents with strong
155 infiltration of T and B cells in the synovium, the diffuse-myeloid pathotype shows
156 predominant influx of myeloid cells and the pauci-immune/fibroid pathotype is
157 characterised by scanty immune cells and prevalent stromal cells(*9*). Consequently,
158 analysis of synovial cell proportions by single cell RNA sequencing (scRNAseq)
159 showed substantial expansion of T- and B-cell compartments in wrist compared to
160 knee RA synovium (Figure 1D and Table 1). In summary, all these data pointed
161 towards higher inflammatory activity in hand versus knee RA synovium.

162 We then used the scRNAseq data to assess whether these site-specific tissue changes
163 were associated with molecular changes in SF. In total, 1,966 genes were differentially
164 expressed in hand and knee SF, 1,026 genes were overexpressed in hand SF and 940
165 in knee SF. We confirmed the joint-specific expression of HOX genes in SF from RA
166 patients in this dataset (Figure 1E). In addition, various pathways that we had

167 previously found to be differentially enriched in cultured hand and knee SF *in*
168 *vitro*(*17*), were also joint-specifically activated *in vivo*, such as cell adhesion,
169 extracellular matrix (ECM) interaction and bone remodeling/osteoclast differentiation
170 pathways (Supplementary Tables S1/S2 and Figure 1F). Several enriched pathways
171 were previously implicated to be relevant in RA such as MAPK, Wnt and PI-Akt
172 signaling(*26*). Additionally, knee SF showed increased levels of *HLA* and *CD74* genes
173 ('Antigen processing and presentation' and 'Rheumatoid arthritis' pathways). Thus,
174 these results confirmed joint specific gene expression in SF in terms of developmental
175 as well as inflammatory pathways.
176 We then sought to understand in how far the joint specific expression of HOX
177 transcripts was involved in these site-specific gene expression changes. To this end,
178 we silenced SF for *HOXD10*, *HOXD11*, *HOXD13*, and the long non-coding RNAs
179 *HOTAIR* and *HOTTIP*, respectively. These HOX transcripts were the most
180 discriminating transcripts in cultured SF and synovial tissues between the hand and
181 knee in our previous *in vitro* analysis(*17*). Due to the lower sequence depths in
182 scRNAseq, the less expressed transcripts *HOXD13*, *HOTTIP* and *HOTAIR* were not
183 detectable in the scRNAseq dataset (Figure 1E). The differential gene expression by
184 *HOX* gene silencing *in vitro* corresponded to 70.9% of the differential gene expression
185 between the hand and knee *in vivo* using scRNAseq (Figure 1G). Among the different
186 *HOX* genes, *HOTAIR* alone regulated almost 49.3% of this joint-dependent gene
187 expression. This suggested that joint-specific expressed HOX transcription factors and
188 non-coding RNAs drive most of the joint-specific transcriptome in RA SF.
189
190
191

Figure 1: *HOTAIR* regulates site-specific gene expression in synovial fibroblasts

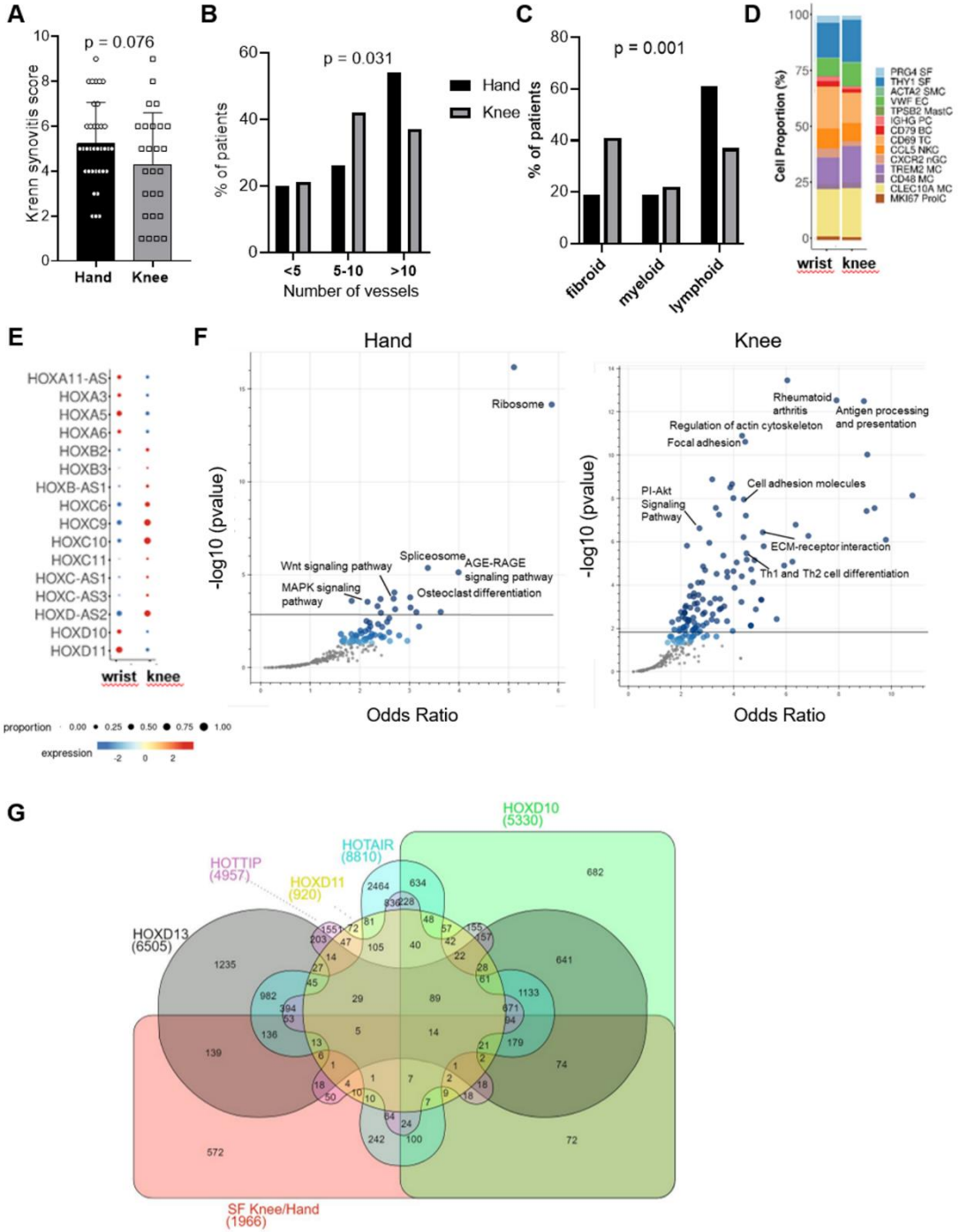

A) Krenn synovitis score in hand (n = 36) and knee (n = 27) synovium from RA patients. Unpaired t test. Mean +/- standard deviation is shown. **B)** Vascularization as assessed by CD31staining in synovium from RA patients (35 hands and 24 knees). Vessels were counted in 5 fields (20x magnification). Chi squared test. **C)** Synovial pathotype in 36 hand and 27 knee RA synovium, Chi squared test. **D)** Cell proportions between hand (n = 8) and knee (n = 4) synovium using single cell RNA sequencing. SF: synovial fibroblasts, SMC: smooth muscle cells, EC: endothelial cells, MastC: mast cells, PC: plasma cells, BC: B cells, TC: T cells, NKC: NK cells, nGC: neutrophilic granulocytes, MC: myeloid cells, ProIC: proliferating cells. **E)** HOX gene expression in hand (n = 8) and knee (n = 4) synovial fibroblasts from RA patients in single cell RNA sequencing analysis. **F)** Scatter dot plot of pathway enrichment analysis of genes significantly enriched in hand SF (n = 8) and in knee SF (n = 4) (FDR < 0.05; Log fold change +/-1). Blue dots: significantly enriched pathways, darker color corresponds to lower p-values. Grey dots represent pathways with p > 0.05. **G)** Overlap between genes regulated by *HOX* genes (*HOXD10*, *HOXD11*, *HOXD13*, *HOTTIP*, *HOTAIR*) and genes differentially expressed between hand (n = 8) and knee (n = 4) SF in single cell RNA sequencing. Intersection was assessed using Venn diagram. SF: synovial fibroblasts.

207 Table 1: Patient's characteristics single cell RNA sequencing of RA patients

	Wrist/metacarpophalangeal joint (n=8)	Knee (n=4)
Age (yrs)	59.6 ± 12.0	58.5 ± 19.2
Female (n)	6	4
RF or anti-CCP positivity (n)	5	2 (n=1 with missing information)
Previous biological treatment (n)	7	3 (n=1 with missing information)
Disease modifying treatment at the time of the biopsy (n)	3	0 (n=1 with missing information)

208 Yrs: years, RF: rheumatoid factor, RA. Rheumatoid arthritis

209 **Joint and disease specific expression of *HOTAIR***

210 We previously showed that *HOTAIR* is exclusively expressed in lower limb SF and
211 joints in both mice and human(*17*). By in situ hybridisation (ISH), we confirmed that
212 *HOTAIR* is expressed in synovial tissues from knees (Figure 2A), but not from hands
213 (Figure 2B). In the synovium, *HOTAIR* was expressed mainly in SF, in both the lining
214 and the sublining synovium (Figure 2C). Analysis of *HOTAIR* expression in knee
215 joints of OA and RA patients showed that *HOTAIR* was significantly more abundant
216 in OA than in RA knees (Figure 2D/E). The difference in *HOTAIR* expression between
217 OA and RA was lost in cultured knee SF (p=0.133) (Figure 2F), suggesting that the
218 lower expression of *HOTAIR* in RA joints was modulated by local factors *in vivo*.

219

220

221

222

Figure 2 *HOTAIR* is expressed in synovial tissues of lower extremity joints with higher expression in OA than in RA.

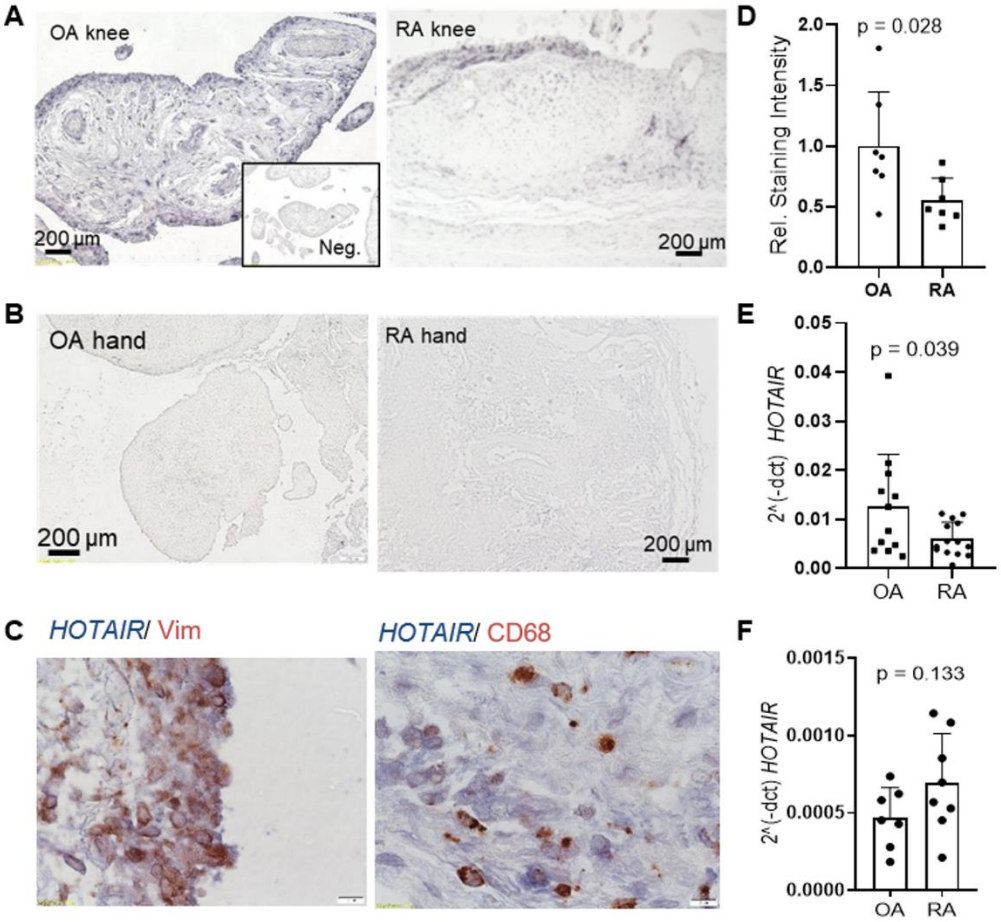

A) Representative pictures of synovial tissues from knee joints of OA (left, n = 6) and RA (right, n = 5) patients stained for *HOTAIR* by in-situ hybridization (ISH). Magnification 100x. Inset shows staining with the anti-sense probe (negative control). **B)** Representative picture of *HOTAIR* in-situ hybridization in synovial tissues of OA and RA hand joints (n = 3). Magnification 100x. **C)** Double staining of *HOTAIR* (in blue) and vimentin (in red, left panel) or CD68 (in red, right panel) to assess *HOTAIR* expression in synovial fibroblasts and macrophages, respectively. Magnification 400x. **D)** Relative quantification of *HOTAIR* ISH in OA and RA synovial tissue using ImageJ. Unpaired t test. **E)** Expression of *HOTAIR* measured by quantitative PCR in OA and RA synovial tissues. Unpaired t test. **F)** Expression of *HOTAIR* measured by quantitative PCR in cultured OA and RA SF. Unpaired t test. SF: synovial fibroblasts, OA: osteoarthritis, RA: rheumatoid arthritis. dct: cycle of threshold target – cycle of threshold housekeeping gene. Mean +/- standard deviation is shown.

To determine which local factors could influence the expression of *HOTAIR* in arthritis, we assessed *HOTAIR* expression in SF upon stimulation by various cytokines and Toll-like receptor (TLR) ligands. Stimulation with most of the inflammatory cytokines decreased *HOTAIR* expression in SF (Figure 3A). Furthermore, active promoter and enhancer sites at the *HOTAIR* locus were closed after TNF stimulation (Figure 3B). Consistently, *HOTAIR* expression inversely correlated with *TNF*

243 expression in arthritic synovium (Figure 3C). SF isolated from arthritic, TNF
244 transgenic mice (TG197) expressed lower levels of *Hotair* than SF from healthy wild-
245 type mice (Figure 3D), showing that the down-regulation of *HOTAIR* in inflammatory
246 conditions is conserved across species.

247 ***HOTAIR* regulates arthritis relevant pathways**

248 We next examined the effect of downregulation of *HOTAIR* in inflammatory states in
249 SF. Since *HOTAIR* represses gene expression by placing repressive H3K27me3
250 marks(*19*), we first analysed the effect of *HOTAIR* downregulation in SF on
251 H3K27me3. A total of 2,376 genomic sites with differential presence of H3K27me3
252 marks were identified between control SF and SF silenced for *HOTAIR*. The frequency
253 of repressive H3K27me3 marks was decreased in promoters near transcription start
254 sites in *HOTAIR*-silenced SF, showing a clear impact of *HOTAIR* downregulation on
255 the epigenetic landscape of SF (Figure 3E).

256

257

258

259

260

261

Figure 3. *HOTAIR* is downregulated by inflammatory cytokines and shapes the epigenetic landscape of SF.

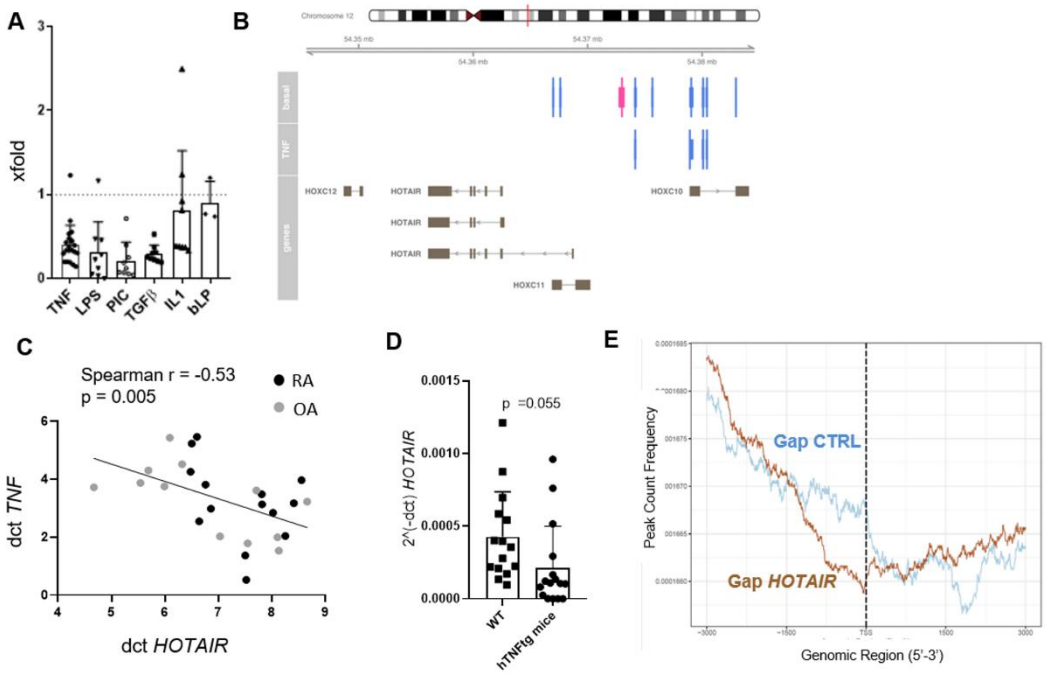

A) SF were left untreated or stimulated with TNF, LPS, poly I:C (PIC), TGFβ, IL1β, or bacterial lipoprotein (bLP) for 24 hours. Expression of *HOTAIR* was measured by qPCR. $P < 0.001$ for TNF, LPS, PIC and TGFβ. IL1β and bLP $p > 0.05$. Unstimulated samples were set to 1. **B)** CAGE analysis of enhancers/promoters at the HOTAIR locus in SF from knees (n = 2) in basal conditions and after stimulation with TNF. After TNF stimulation several active promoters (light blue bars) and the enhancer (pink bar) disappear in knee SF. **C)** Correlation between *TNF* and *HOTAIR* expression measured by qPCR in RA synovial tissues and analysed by Spearman correlation. **D)** Expression of *Hotair* was measured by qPCR in ankle SF isolated from wildtype (WT) and TNF transgenic (Tg197) C57BL/6 mice and analysed by unpaired t test. **E)** ChIP sequencing of H3K27me3 marks in SF silenced for *HOTAIR* (n = 3) and control SF (n = 3) was performed 48h after transfection. TSS: Transcription start site. SF: synovial fibroblasts, RA: rheumatoid arthritis, OA: osteoarthritis, dct: cycle of threshold target – cycle of threshold housekeeping gene. Mean +/- standard deviation is shown.

We then investigated the transcriptional changes associated with *HOTAIR* silencing in SF, mimicking an inflammatory arthritis environment. A total of 7,885 genes were differentially expressed between control and *HOTAIR*-silenced SF (FDR < 0.05), with enrichment of site-specific signaling pathways such as MAPK, Wnt and PI-Akt signaling (Figure 4A, Supplementary Table S3). RNA and ChIP sequencing suggested a *HOTAIR*-dependent regulation of several collagen transcripts, including *COL1A1*, *COL1A2* and *COL3A1*, which could, however, not be confirmed by quantitative PCR (Figure 4B). In contrast, there was a trend towards increased procollagen release into supernatants from *HOTAIR*-silenced SF (Figure 4C). Assuming that prolonged 3D culture systems provide a more natural environment for

285 the production of extracellular matrix proteins from fibroblasts, we cultured control
286 and *HOTAIR*-silenced SF in 3D micromass organ systems. After 3 weeks in culture,
287 *HOTAIR*-silenced SF had deposited significantly more collagen-1 in micromasses
288 compared to control SF (Figure 4D). Consistent with an increase in extracellular
289 matrix remodelling in *HOTAIR*-silenced micromasses, several transcripts of the
290 fibroblast growth factor (FGF) family, known to play a key role in extracellular matrix
291 remodelling (*27*), were regulated by *HOTAIR*, albeit most of them were down-
292 regulated. However, a particular strong upregulation of *FGF8* after *HOTAIR* silencing
293 was observed (Figure 4E). FGF were previously shown to signal via the PI-Akt and
294 the Wnt signaling pathway and to play a crucial role in limb development(*28, 29*).
295 Measurements of the expression of AKT and its active phophorylated form showed
296 that *HOTAIR* silencing did not influence AKT levels, but resulted in increased AKT
297 phosphorylation (Figures 4F). Furthermore, we confirmed that silencing of *HOTAIR*
298 regulated several transcripts in the Wnt signaling pathway (Figure 4G) and repressed
299 the activation of the canonical Wnt pathway in SF (Figure 4H). Finally, we confirmed
300 that *HOTAIR* regulated several cytokines and transcription factors which were
301 previously implicated in SF activation in RA (*IL-12*(*30*), *IL-6*(*31*), *CXCL12*(*32*),
302 *PTEN*(*33*), *FOXO1*(*34*), *RUNX1*(*35*)) (Figure 4I). IL-12 and IL-6 secretion by SF
303 increased after the silencing of *HOTAIR*, while CXCL12 secretion decreased (Figure
304 4J). Increased IL-6 levels were also released by micromasses formed with *HOTAIR*
305 silenced SF compared to control SF (Figure 4K). Taken together, these data clearly
306 show that *HOTAIR* can regulate pathways relevant to joint inflammation and tissue
307 remodelling in SF. Inhibition of protein translation did not influence the effect of
308 *HOTAIR* silencing on *CTNNB1*, *FGFR2* and *LGR5* (Supplementary Figure S1A), but
309 suppressed the effect of *HOTAIR* silencing on *GSK3B* and *FGF7* (Supplementary

310 Figure S1B), suggesting direct as well as indirect mechanims (e.g. mediated by an

311 intermediate protein) of this regulation.

312 **Figure 4. *HOTAIR* modulates arthritis relevant pathways.**

313

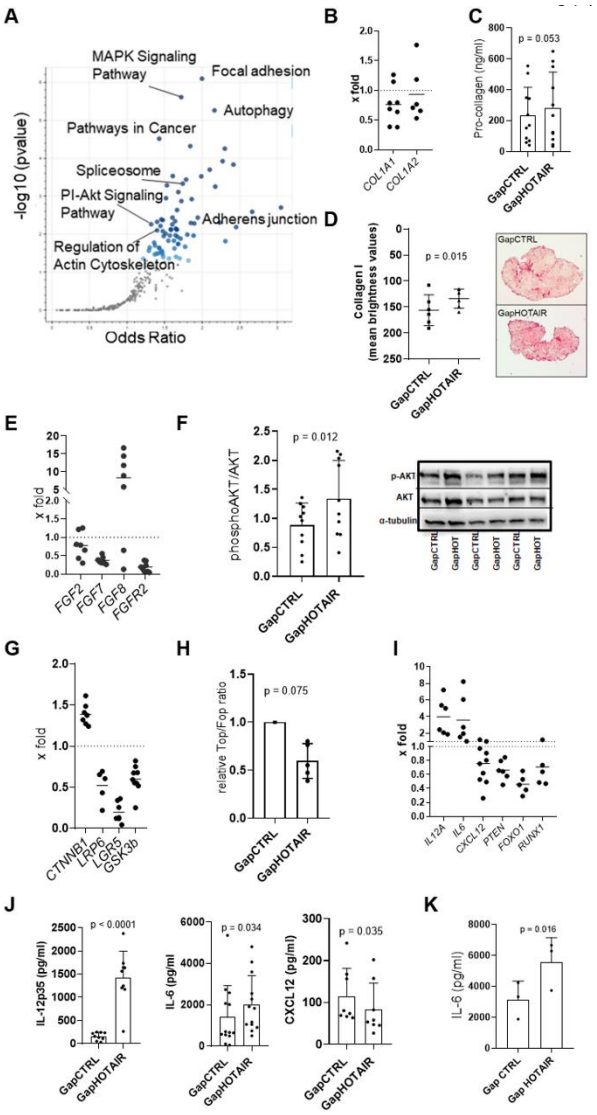

A) Scatter dot plot of pathway enrichment analysis of genes significantly changed after *HOTAIR* silencing (FDR < 0.05; Log fold change +/-1). Blue dots: significantly enriched pathways, darker color corresponds to lower p-values. Grey dots represent pathways with p > 0.05. **B)** Expression of *COL1A1* and *COL1A2* measured by quantitative PCR between SF transfected with control or *HOTAIR* targeting GapmeR after 48h. Control transfected cells were set to 1. **C)** Pro-Collagen was measured in supernatants of SF transfected with control or *HOTAIR* targeting GapmeR after 72h by ELISA. Paired t test. **D)** Collagen I was stained by immunohistochemistry in 3D micromasses formed with control or *HOTAIR* silenced SF. Right panel: representative pictures, 25x magnification; left panel: quantification with ImageJ and analysis with paired t test. **E)** Expression of *FGF2*, *FGF7*, *FGF8* and *FGFR2* measured by quantitative PCR between SF transfected with control or *HOTAIR* targeting GapmeR after 48h. Control transfected cells were set to 1. **F)** Expression of AKT and phosphorylated AKT in SF transfected with control or *HOTAIR* targeting GapmeR after 72h. Right panel: representative examples; left panel: densitometric analysis. Paired t test. **G)** Expression of *CTNNB1*, *LRP6*, *LGR5* and *GSK3B* measured by quantitative PCR between SF transfected with control or *HOTAIR* targeting GapmeR after 48h. Control transfected cells were set to 1. **H)** Activation of the canonical Wnt pathway was assessed by luciferase assay with a Wnt reporter gene (Top) or a mutated Wnt reported gene (Fop) as control in SF transfected with control or *HOTAIR* targeting GapmeR after 48h. One sample t test. **I)** Expression of *IL12A*, *IL6*, *CXCL12, PTEN, FOXO1* and *RUNX1* measured by quantitative PCR between SF transfected with control or *HOTAIR* targeting GapmeR after 48h. Control transfected cells were set to 1. **J)** Selected proteins were measured in supernatants of SF transfected with control or *HOTAIR* targeting GapmeR after 48h (CXL12) or 72h (IL-6, IL-12-p35) by ELISA. Paired t test. **K)** IL-6 was measured in supernatants of micromasses after 3 weeks by ELISA. Paired t test. Data are representative for at-least 2 experiments. Mean +/- standard deviation is shown.

357

358 **Changes in *HOTAIR* expression modulate SF subtypes**

359 Since several marker genes for recently described SF subpopulations(*15, 36-38*) were

360 affected by *HOTAIR* silencing, we wondered whether the observed transcriptional

361 changes after *HOTAIR* silencing might be connected to changes in the proportion and

362 the formation of SF subtypes. Four subpopulations of SF have been described by

363 scRNAseq (*15, 36-38*): PRG4^{+} SF are considered as lining SF, CXCL12^{+} SF are

364 characterised by increased expression of *CXCL12*, *CD74* and *IL-6*, POSTN^{+} SF show
365 high production of extracellular matrix proteins such as collagens and periostin, and
366 CXCL14^{+} SF are CD34^{+} SF. We integrated scRNAseq data from control and
367 *HOTAIR*-silenced SF cultures with our previous meta-analysis of synovial tissue
368 scRNAseq data from five different datasets(*38*) (Figure 5). In line with published data,
369 PRG4^{+} SF and CXCL12^{+} SF subtypes were partially lost during culture (Figure
370 5B)(*14*). The main SF subpopulations in culture were POSTN^{+} SF, CXCL14+ SF, and
371 a mixed-marker cell population consisting of proliferating cells (prolSF) (Figures 5A-
372 E). Silencing of *HOTAIR* indeed resulted in a shift in the distribution of SF
373 subpopulations with an enrichment in PRG4^{+} SF and a decrease in POSTN^{+} SF (Figure
374 5C). *COL1A1* and *COL1A2* expression was mainly increased in PRG4^{+} SF, with no
375 change or a decrease in POSTN^{+} SF (Figure 5F): This might reflect a transcriptional
376 switch from POSTN^{+} SF to collagen producing PRG4^{+} SF and might explain the
377 inconsistent results seen in the bulk analysis of COL transcripts (Figure 4B). *CXCL12*
378 downregulation was found in CXCL14^{+} SF, which produce *CXCL12,* but to a lesser
379 extent than CXCL12^{+} SF (Figure 5D/E/F). *IL-6* upregulation was observed across all
380 SF subtypes (Figure 5F). From this analysis, we concluded that *HOTAIR* played a role
381 in the formation of SF subtypes, for example, by regulating differential collagen
382 production between the SF subtypes. However, there were also regulatory mechanisms
383 of *HOTAIR* that were evident in all SF subtypes.
384
385
386
387
388

389 **Figure 5. Changes in *HOTAIR* expression modulate SF subtypes.**
390

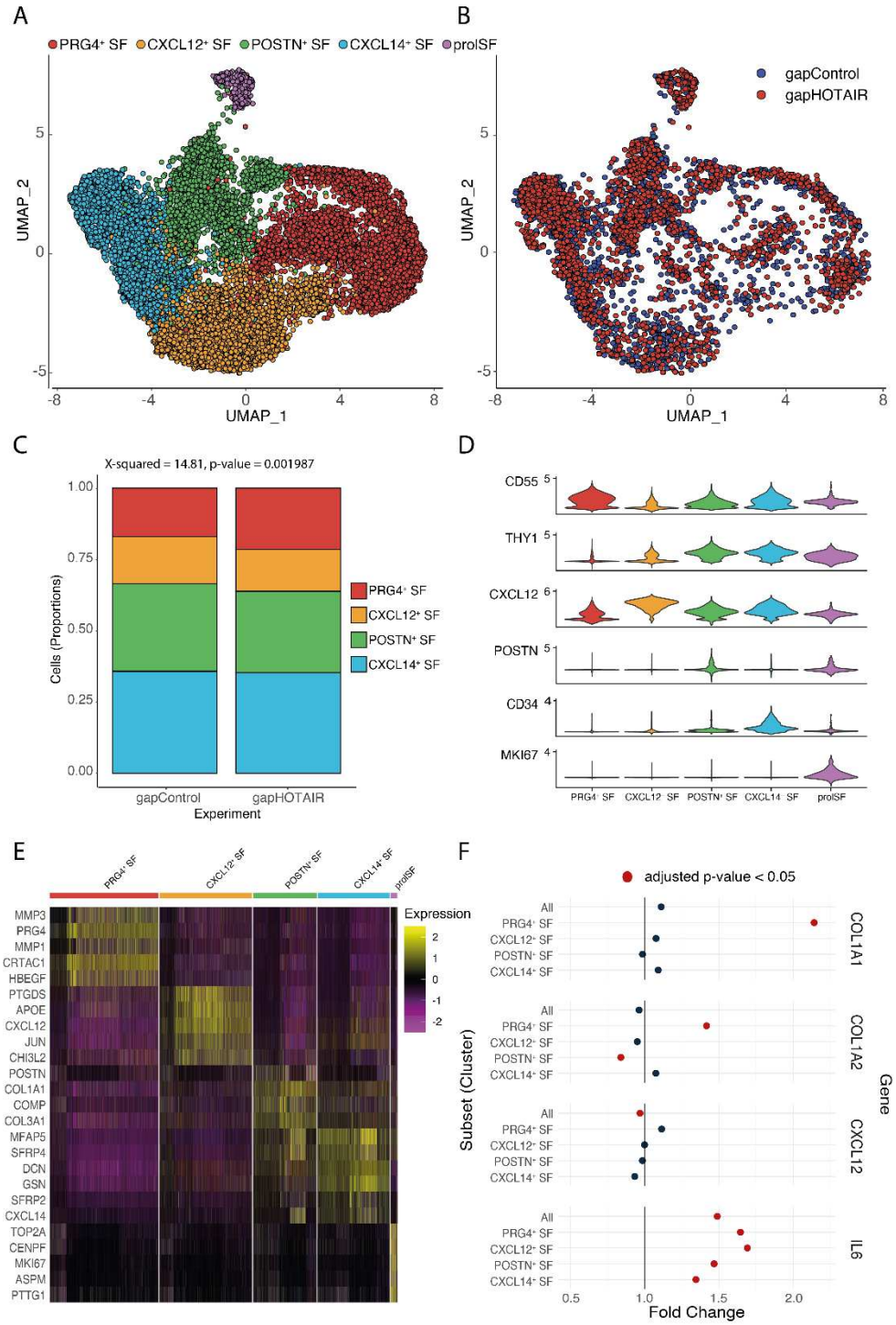

411 **A)** Single cell RNA sequencing (scRNAseq) data from synovial tissues were integrated with scRNAseq data from cultured SF
412 transfected with control or *HOTAIR* targeting GapmeR (n = 3). UMAP representation of the different SF subtypes is shown. **B)**
413 UMAP representation of the distribution of cells in control and *HOTAIR* silenced SF (cultured cells only). **C)** Proportions of the
414 different SF subtypes in control and *HOTAIR* silenced SF. **D)** Selected marker gene expression in the different SF subtypes. **E)**
415 Heatmap with the top 5 marker genes for each subtype**. F)** Change of expression of selected genes within the different SF
416 subtypes.
417

418

419 ***HOTAIR* downregulation alters key functions in SF and surrounding cells**

420 Next we aimed to decipher the functional changes of SF induced by *HOTAIR*
421 downregulation upon inflammation. Real-time analysis of attachement and growth of
422 SF *in vitro* did not show any changes in adhesion (Figure 6A) and proliferation (Figure
423 6C), but a decrease in spreading of *HOTAIR* silenced SF (Figure 6B). Accordingy,
424 silencing of *HOTAIR* resulted in decreased migration of SF (Figure 6D and Movie 1).
425 These data are in line with the findings that *HOTAIR* regulated genes were enriched
426 in the pathways "actin cytoskeleton" and "Wnt signaling" (Table S3 and Figure 4G/H),
427 which were previously linked to tissue remodelling and cell migration(*39, 40*).
428 Furthermore, *HOTAIR* silencing increased Fas-induced apoptosis in SF (Figure 6E),
429 as also indicated by the pathway ('apoptosis') in the pathway analysis (Table S3).
430 Since osteoclastogenesis is of major importance in RA and was differentially
431 expressed between hand and knee SF (Table S2), we assessed the effect of silencing
432 *HOTAIR* in SF on osteoclastogenesis and osteoclast function. Co-culture of
433 differentiating monocytes with *HOTAIR* silenced SF, but not the addition of
434 supernatants from *HOTAIR* silenced SF, decreased osteoclast formation (Figure 6F),
435 suggesting that cell-cell contact was needed to inhibit osteoclastogenesis. In contrast,
436 osteoclasts in co-culture with *HOTAIR* silenced SF, as well as incubated with
437 supernatants showed decreased osteoclast activity, which could be an effect of
438 decreased secretion of CXCL12 by *HOTAIR* silenced SF(*41*) (Figure 6G).

439

440

441

442

443

Figure 6. *HOTAIR* silencing induces functional changes in SF.

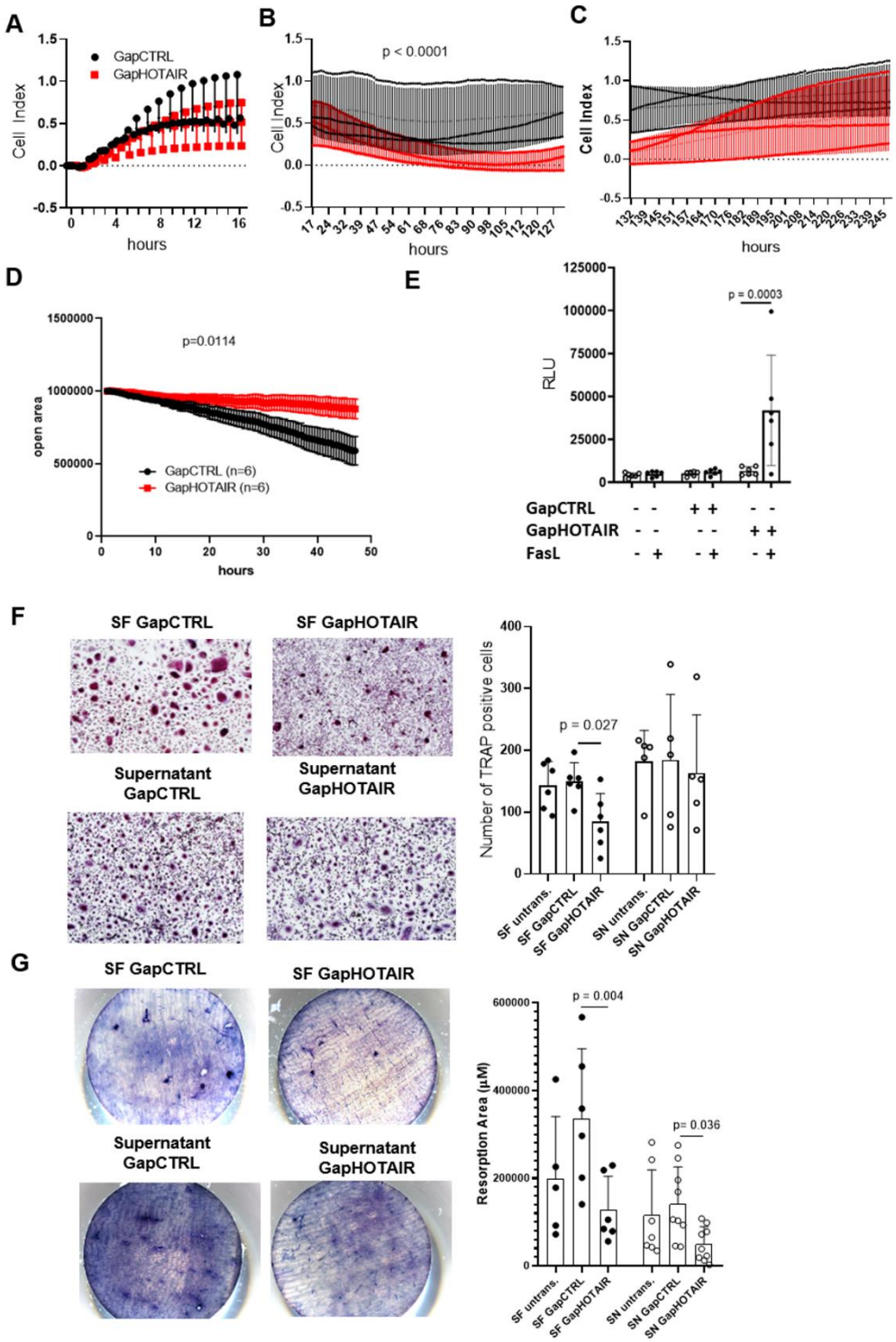

Real-time measurements of SF **A)** adhesion (0-16 h), **B)** spreading (17-127 h) and **C)** proliferation (132-245 h) in *HOTAIR* silenced and control SF (n = 3). Two-way ANOVA. **D)** Measurement of open area covered over time by control SF or *HOTAIR* silenced SF (n = 6) in scratch assay. Two-way ANOVA. **E)** Caspase 3/7 activation in untransfected, control and *HOTAIR* GapmeR transfected SF after 48h of transfection. RLU = relative luminescence units after background subtraction. One-way ANOVA with Bonferroni's correction. **F)** Left panel: representative pictures of tartrate-resistant acid phosphatase (TRAP) staining of osteoclasts differentiated from monocytes by co-culture (upper panel) or incubation with supernatants (SN) of control or *HOTAIR* transfected SF (lower panel). Magnification 400 x. Right panel: Quantification of TRAP+ cells in the described conditions. Paired t test with Bonferroni correction. **G)** Left panel: representative pictures of resorption areas after incubation of bone slices with osteoclasts differentiated by co-culture (upper panel) or incubation with supernatants of control or *HOTAIR* transfected SF (lower panel). Right panel: Quantification of resorption areas in the described conditions. Paired t test with Bonferroni correction. The results are representative for at-least 2 experiments. Mean +/- standard deviation is shown.

457 Since the levels of several chemokines and cytokines were affected by *HOTAIR*
458 silencing (Supplementary Table S3), we compared the chemotactic activity of
459 supernatants derived from control or *HOTAIR* silenced SF. Despite a similar amount
460 of healthy peripheral blood mononuclear cells (PBMCs) migrating towards
461 conditioned supernatants from controls and *HOTAIR* silenced SF (Figure 7A), we
462 observed a shift in the cellular composition of the migrated PBMCs with an increased
463 number of CD19+ B cells (Figure 7B) and a decreased number of CD14+ monocytes
464 (Figure 7C) using supernatants from *HOTAIR* silenced SF. A slight increase was also
465 seen for the chemotaxis of CD3+ T cells (Figure 7D). In line with these results,
466 synovia of RA and OA patients with low *HOTAIR* expression were characterized by
467 higher CD20+ B cell (Figure 7E) and, in particular, CD138+ plasma cell infiltration
468 (Figure 7F) and a lymphoid pathotype (Figure 7G). Consistently, in the early RA
469 cohort (PEAC) (PEAC (qmul.ac.uk))(*42*), a low synovial *HOTAIR* expression in
470 synovium was associated with a trend towards a lymphoid pathotype (Figure 7H) and
471 *HOTAIR* expression was negatively correlated with CD138+ plasma cell infiltrates (r:
472 0.27, padj: 0.023) (Figure 7I). In summary, these data support the notion that
473 expression levels of *HOTAIR* in SF can shape the influx of immune cells in the
474 synovium in arthritis and vice-versa.

475 ***HOTAIR* site-specific expression may shape inflammatory response in other**
476 **organs**

477 Since HOX gene expression is site specifically expressed in stromal cells of several
478 organs and tissues, we wondered whether *HOTAIR* might shape the inflammatory
479 response in other tissues than joints. Site-specific expression of *HOTAIR* was already
480 shown in human skin where it also follows the upper vs lower body part pattern(*18*).
481 In addition, we measured site-specific expression of *Hotair* in mouse spine and found

482 increased expression in lumbal compared to cervical spine (p = 0.009) (Figure 7J).
483 Furthermore, in the different anatomic compartments of the gastrointestinal tract,
484 *Hotair* showed site-specific expression with higher expression in the distal parts of the
485 intestines compared to stomach and the small intestines (Figure 7K).

486 **Figure 7. *HOTAIR* silencing increases lymphocyte chemotaxis.**

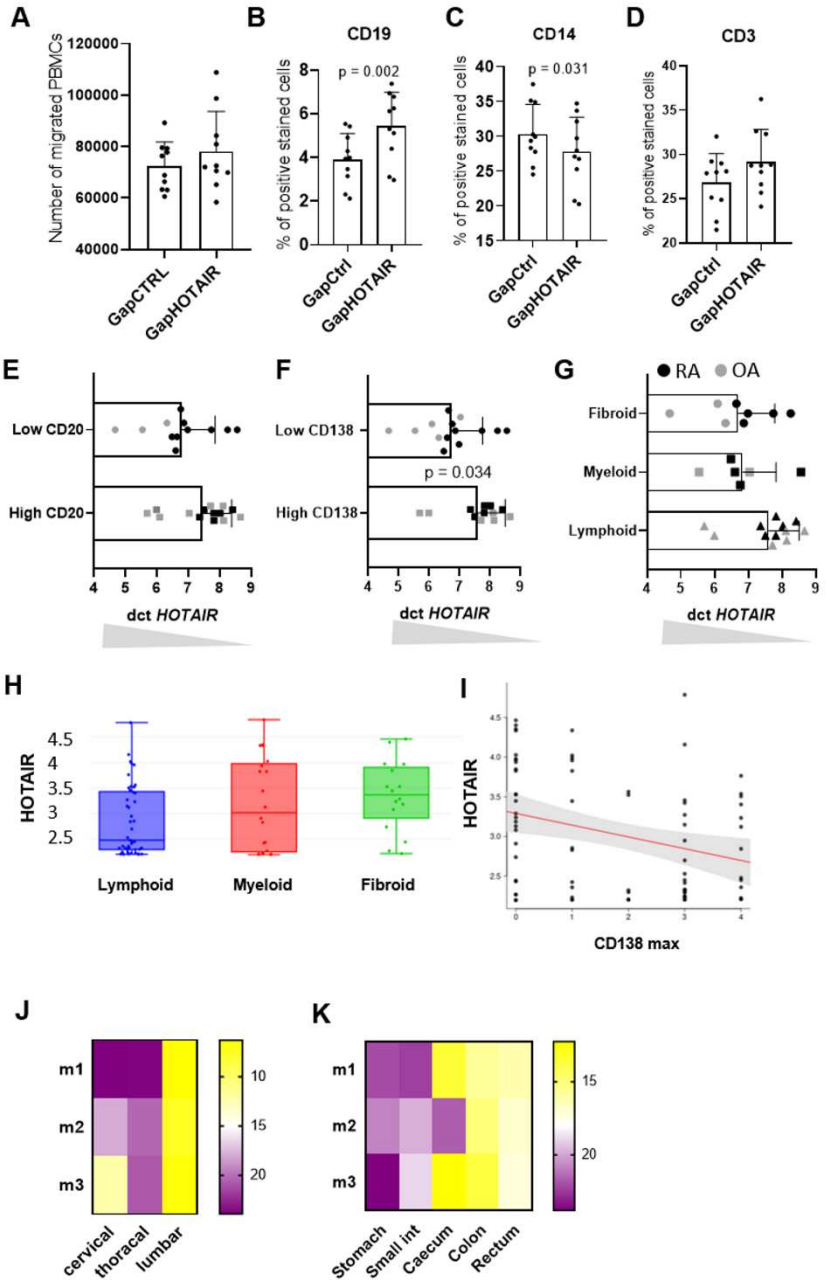

508

509 **A)** The amounts of PBMCs migrating through a transwell system towards conditioned supernatants from SF transfected with
510 control GapmeR or *HOTAIR* GapmeR. Paired t test, p = 0.19. **B-D)** The percentage of **B)** CD19, **C)** CD14 and **D)** CD3 positive
511 cells was measured in PBMCs that had migrated towards supernatants of control or *HOTAIR* silenced SF. Paired t test. **E-G)**
512 Expression levels of *HOTAIR* were measured by qPCR in synovial tissues from rheumatoid arthritis (RA) and osteoarthritis (OA)
513 with **E)** high (CD20+ score ≥ 2) or low amounts of CD20+ B cells (unpaired t test, p = 0.10), **F)** with high (CD138+ score ≥ 2)
514 or low amounts of CD138+ plasma cells (unpaired t test), **G)** with pauci-immune, myeloid or lymphoid pathotypes (one-way
515 Anova, p = 0.11). dct: cycle of threshold target – cycle of threshold housekeeping gene. **H-I)** Expression levels of *HOTAIR* in

RNA sequencing in synovial tissues from the PEAC cohort according to **H)** the synovial pathotype and to **I)** CD138 infiltrates. **J-K)** Expression of *Hotair* was measured by qPCR in C57/BL6 mice (n = 3) **J)** in cervical, thoracal and lumbal spine and in **K)** different parts of the gut (stomach, small intestine, caecum, colon and rectum). Heatmap of the dct of *HOTAIR* expression according to the localisation are presented. Mean +/- standard deviation is shown.

DISCUSSION

Here, we show that *HOTAIR* is a major regulator of site-specific gene expression in SF and modulates a series of highly relevant signalling pathways and SF functions in arthritis. *HOTAIR*-modulated changes in SF gene expression and function were associated with changes betweeen hand and knee arthritis in RA, suggesting that *HOTAIR* may shape the phenotype of arthritis in lower extremity joints. By showing that an embryonically imprinted, site-specific factor can regulate inflammation-related signalling pathways, our data support the concept that anatomically defined features of the local stroma can influence the susceptibility and manifestation of inflammation. Here, we showed that *HOTAIR* expression in SF is decreased after stimulation by local inflammatory factors, which could explain this decreased expression in RA SF. Other recent studies have shown that *HOTAIR* expression could be regulated by various factors in the local microenvironment, such as hypoxia(*43*), hormons(*24*) or inflammatory factors(*44*).

The ability of external factors to influence *HOTAIR* expression supports the idea that embryonic site-specific expression of *HOTAIR* is used to trigger a locally distinct and anatomically restricted stress response. Interestingly, it has been suggested that *HOTAIR* may also be mechanoresponsive in response to stretch(*45*). Given the increased expression of *HOTAIR* in the lower limbs and lumbar spine, load and mechanosensing could be additional factors that regulate site-specific response pathways via *HOTAIR*.

In our study, inflammation-induced downregulation of *HOTAIR* modulated several inflammatory response pathways in SF, such as the MAPK, PI-Akt and canonical Wnt

544 pathways. Consistent with our results, *HOTAIR* silencing inhibited the canonical Wnt
545 pathway in gastric and pancreatic cancer cells(*46, 47*) and in OA chondrocytes(*48,*
546 *49*). In OA chondrocytes(*49*), *HOTAIR* has been shown to act directly on Wnt
547 inhibitory factor 1 (WIF-1) by increasing histone H3K27 trimethylation in the *WIF-1*
548 promoter, leading to WIF-1 repression that promotes activation of the Wnt/β-catenin
549 pathway. Consistent with this study, our own results based on the adjunction of
550 cycloheximide suggest an indirect mechanism underlying the *HOTAIR*-mediated
551 regulation of the Wnt pathway.
552 Activation of the Wnt pathway is a characteristic of the pauci-immune subtype of
553 synovitis in RA, whereas more inflammatory pathways such as PI-Akt have been
554 found to be activated in lymphoid/myeloid synovial pathotypes(*6, 8, 9*). Consistently,
555 lower levels of *HOTAIR* in synovial tissue were associated with a lymphoid pathotype
556 in our study. Furthermore, *HOTAIR* silencing exerted a chemotactic effect on
557 lymphocytes *in vitro*. Thus, it can be speculated that *HOTAIR* acts as a stromal
558 regulator of the inflammatory tissue response, whose downregulation under conditions
559 with high levels of TNF might promote the development of a lymphocyte-dominated
560 inflammatory response.
561 Studies analysing the differences between RA in different joints are rare. Our results
562 suggest that hand RA is more likely than knee RA to show the classic signs of synovitis
563 described for RA, whereas the fibroid pathotype of synovitis was more common in
564 knee RA than in hand RA. Refractory, difficult-to-treat arthritis has been associated
565 with this non-inflammatory fibroid pathotype (*10*), however, up to now it is not known
566 whether lower limb synovitis is more often resistant to immunosuppressive therapy.
567 In depth analysis of the characteristics of knee RA has suggested severe cartilage
568 destruction but less bone erosion compared to what is known from RA of the hand(*50*).

569 Similarly, OA of the hand tends to be more erosive than OA of the knee(*51*). The less
570 destructive phenotype of RA and OA in knees may be due to protective mechanisms
571 exerted by the joint-specific stroma. Both, our comparison of knee and hand RA as
572 well as our analysis of *HOTAIR* function pointed towards decreased
573 osteoclastogenesis in knees compared to hands. Co-culture of differentiated
574 monocytes with *HOTAIR*-silenced SF, but not the addition of *HOTAIR*-silenced SF
575 supernatants, decreased osteoclast formation, suggesting that cell-cell contact was
576 necessary to inhibit osteoclastogenesis. Thus, the decrease in osteoclastogenesis after
577 *HOTAIR* silencing could be related to the reduced migratory function of SF silenced
578 for *HOTAIR*, which was also observed in another study(*44*). Another explanation is
579 that the decrease in osteoclastogenesis is mediated by the decreased CXCL12 secretion
580 following *HOTAIR* silencing(*52*), as osteoclasts co-cultured with *HOTAIR* silenced
581 SF but also incubated with supernatants showed decreased osteoclast activity(*41*).
582 One limitation of our study is that with the available data we cannot directly show how
583 down-regulation of *HOTAIR* during inflammation affects the inflammatory response
584 in a joint-specific manner. *In vivo* confirmation of our hypotheses is hampered by the
585 fact that *Hotair* does not have the same function in morphological development in
586 mice and humans(*53*), and it is therefore questionable whether the function in
587 regulating inflammatory pathways is conserved. These differences between the
588 species might be explained by biomechanical and anatomical differences between
589 quadrupedal walking in mice versus bipedal walking in humans(*45, 54*). If our
590 hypothesis of an influence of site-specific embryonic factors on inflammatory
591 responses is valid, species-specific differences in limb formation, anatomy and
592 biomechanics may underlie the limited translation of preclinical studies in mice to
593 human arthritis.

594 Beyond the joint, *HOTAIR* appears to be involved in the site-specific regulation of
595 inflammation in other organs. Thus, it has recently been identified as a major regulator
596 of region-specific development of adipose tissue, which is associated with site-specific
597 metabolic complications, with exclusive expression in gluteofemoral subcutaneous
598 adipose tissue (*24, 55*). In addition, *HOTAIR* is mostly expressed in distal dermal
599 fibroblasts(*18*). Consistently, we observed site-specific expression of *HOTAIR* in the
600 spine and intestine with increased expression in the lumbar spine and distal parts of
601 the intestines. In spondyloarthritis, it has been suggested that involvement of the
602 lumbar spine is more frequent(*56*) and more severe with more bone bridges compared
603 to cervical involvement(*57*). Furthermore, Wnt signaling plays a crucial role in the
604 formation of bone bridges in spondyloarthritis(*58*). Similarly, inflammatory bowel
605 disease encompasses two types of idiopathic intestinal disease that are differentiated
606 by their location and the depth of involvement in the bowel wall(*59*). Ulcerative colitis
607 most commonly affects the rectum, whereas Crohn's disease most often affects the
608 terminal ileum and colon. Interestingly, Wnt signaling has been identified as a key
609 regulatory pathway in the intestinal mucosa(*60*). Thus, important future work will be
610 to elucidate whether the site-specific expression of *HOTAIR* underlies the
611 development of site-specific phenotypes of these inflammatory diseases.
612 In conclusion, we suggest that the phenotype and severity of inflammation are
613 modulated by the embryonic imprinted local stromal gene signature. Further
614 investigation into joint specific factors favouring and shaping the development of
615 arthritis will improve understanding of the pathogenesis of arthritis and could lead to
616 the development of specific therapies targeting joint specific signaling pathways.
617

618 **METHODS**

619 **Patients**

620 Synovial tissues were obtained from OA and RA patients undergoing joint
621 replacement surgery at the Schulthess Clinic Zurich, Switzerland or from ultra-sound
622 guided joint biopsies. RA patients fulfilled the 2010 ACR/EULAR (American College
623 of Rheumatology/European League Against Rheumatism) criteria for the
624 classification of RA(*61*) whereas OA was considered in cases of chronic pain and
625 manifest radiographic signs of OA(*62*) without any underlining inflammatory
626 rheumatic disease. Patients' characteristics are given in Table 2.

627 Table 2: Patient's characteristics

In-situ hybridization	OA (n=6)	RA (N=5)
Age (yrs)	65.0 ± 6.9	68.0 ± 8.1
Female (n)	4	5
Disease duration (yrs)		23.0 ± 10.6
Knee, hip, feet	6, 0, 0	5, 0, 0
Positive RF		60%
CRP (mg/L)	2.0 ± 1.9	22.0 ± 30.3
RA treatnent		2 TNF-blocker, 2 steroids, 1 none
qPCR in synovial tissues	OA (n=12)	RA (N=14)
Age (yrs)	69.0 ± 11.5	69.0 ± 12.2
Female (n)	8	12
Disease duration (yrs)		19.0 ± 12.9
Knee, hip, feet	9, 3, 0	10, 1, 3
Positive RF		100%
CRP (mg/L)	2.4 ± 2.6	11.0 ± 14.7
RA treatnent		5 TNF-blocker, 7 csDMARDS, 2 unknown
qPCR in cultured SF	OA (n=7)	RA (N=8)

Age (yrs)	64 ± 8.2	70 ± 10.5
Female (n)	3	5
Disease duration (yrs)		15 ± 16.3
Knee, hip, feet	4, 3, 0	4, 3,1
Positive RF		83%
CRP (mg/L)	2.6 ± 8.0	2.8 ± 6.4
RA treatnent		1 TNF-blocker, 5 csDMARDS,1 steroid, 1 unknown

628 OA: osteoarthritis, RA: rheumatoid arthritis, RF: rheumatoid factor, csDMARDS. Conventional disease modifying drugs
629

630 **Culture of SF**

631 *Human* SF

632 Synovial tissues were digested with dispase (37 °C, 1 h) and SF were cultured in
633 Dulbecco's modified Eagle's medium (DMEM; Life Technologies) supplemented
634 with 10% fetal calf serum (FCS), 50 U ml^{-1} penicillin/streptomycin, 2 mM L-
635 glutamine, 10 mM HEPES and 0.2% amphotericin B (all from Life Technologies). For
636 functional assays, vitamin C (50 µg/ml) was added to the culture medium. Purity of
637 SF cultures was confirmed by flow cytometry showing the presence of the fibroblast
638 surface marker CD90 (Thy-1) and the absence of leukocytes (CD45), macrophages
639 (CD14; CD68), T lymphocytes (CD3), B lymphocytes (CD19) and endothelial cells
640 (CD31). Cell cultures were negative for mycoplasma contamination as assessed by
641 MycoAlert mycoplasma detection kit (Lonza). SF from passages 5 to 8 were used.

642 *Murine SF*

643 Primary mouse SF were isolated and cultured for four passages, as previously
644 described (*63*).

645 **Histological analysis**

646 Formalin-fixed, paraffin-embedded synovial tissues of RA or OA patients were cut,
647 put on slides and stained with hematoxylin/eosin. 36 synovial tissues from hands (22
648 from joint replacement and 14 from synovial biopsies) and 27 from knee (18 from
649 joint replacement and 9 from synovial biopsies) were assessed. Synovitis score was
650 assessed by evaluation of the thickness of the lining cell layer, the cellular density of
651 synovial stroma and leukocyte infiltration as described by Krenn *et al.*(*25*).
652 Vascularization was assessed by counting the amount of CD31+ cells on 5 consecutive
653 pictures on 20x objective. Synovial tissue were stained with CD3 (ab16669; Abcam),
654 CD4 (ab183685; Abcam), CD8 (ab22378; Abcam), CD31 (ab28364; Abcam), CD20
655 (M075501-2, Agilent), CD138 (Clone MI15, Agilent) and CD68 (M081401; Dako),
656 to stratify them into lymphoid, myeloid and fibroid pathotypes according to previously
657 published histological features(*7, 9, 25*).

658 **Gene silencing**

659 Hand SF were transfected with 50 nM antisense LNA *HOXD10* (Qiagen, Sequence:
660 5′-TGT CTG CGC TAG GTG G-3′), *HOXD11* (Qiagen, Sequence: 5′-TGC TAG CGA
661 AGT CAG A-3′), *HOXD13* (Qiagen, Sequence: 5′-CAT CAG GAG ACA GTA T-3′)
662 or *HOTTIP* (*HOTTIP*1 Qiagen, Sequence: 5′-TCG GAA AAG TAA GAG T-3′ and
663 *HOTTIP*2 Qiagen, Sequence: 5′-TAC CTA AGT GTG CGA A-3′) GapmeR. Knee SF
664 were transfected with 50 nM antisense LNA *HOTAIR* GapmeR (Qiagen, Sequence:
665 5′-AGG CTT CTA AAT CCG T-3′). Transfections were performed using
666 Lipofectamine 2000 (Invitrogen) according to the manufacturer's instructions.
667 Antisense LNA GapmeR Negative Control A (Cat No 300610) was used as
668 transfection control.

669 **Single-cell RNA sequencing**

670 *scRNAseq of hand and knee synovial tissues*

671 ScRNAseq sequencing was performed on ultrasound-guided joint biopsies of hand (n
672 = 8) or knee (n = 4) joints of RA patients (Patient's characteristics in Table 1). Tissues
673 were processed as previously described(*38*). In brief, tissues were mechanically
674 minced and enzymatically digested using Liberase TL (Roche). 10'000 unsorted
675 synovial cells (viability >80%) per patient were prepared for single cell analysis using
676 the Chromium Single Cell 3' GEM, Library and Gel Bead Kit v3.1, the Chromium
677 Chip G Single Cell Kit and the Chromium controller (all 10x Genomic). Libraries
678 were sequenced on the Illumina NovaSeq6000 instrument to a sequence depth of
679 20,000 to 70,000 reads per cell. CellRanger (v2.0.2) from 10x Genomics was used to
680 demultiplex, align the reads to Ensembl reference build GRCh38.p13 and collapse
681 unique molecular identifiers (UMIs). The standard Seurat protocol(*64*) was used for
682 further analysis. Gene expression between hand and knee was compared. Pathway
683 enrichment analyses of genes differentially expressed between SF from hands and
684 knees were performed using Enrichr (all genes with FDR < 0.05, log fold change +/-
685 1) (*65*). The scatter dot plots were created with the Enrichr Appyter.

686 *scRNAseq of control SF and SF silenced for HOTAIR*

687 scRNAseq in cultured SF transfected with either control or *HOTAIR* targeting
688 GapmeR (n = 3) (Patient's characteristics in Table 3) was performed. SF were washed
689 and counted on a LUNA automated cell counter (Logos Biosystems). 15'000 unsorted
690 SF (viability 60-88%) per patient were prepared for single cell analysis using the
691 Chromium Single Cell 3' GEM, Library and Gel Bead Kit v3.1, the Chromium Chip
692 G Single Cell Kit and the Chromium controller (all 10x Genomic). Libraries were
693 sequenced on the Illumina NovaSeq6000 instrument to a sequence depth of 20,000 to
694 70,000 reads per cell. CellRanger (v2.0.2) from 10x Genomics was used to
695 demultiplex, align the reads to Ensembl reference build GRCh38.p13 and collapse

696 unique molecular identifiers (UMIs). scRNAseq for control SF and SF silenced for
697 HOTAIR were integrated with SF of publicly available datasets (*15, 36, 37, 66*) and
698 two in-house datasets(*38*). The standard Seurat (version 4.0) protocol(*64*) was
699 followed for analysis. Quality control included the exclusion of cells with >25%
700 mitochondrial reads and <5% ribosomal reads; exclusion of mitochondrial, ribosomal
701 and hemoglobin genes and inclusion of only cells with at least 200 detected genes. For
702 the integration of all datasets, we applied harmony(*67*) within the standard Seurat
703 workflow and performed the analysis as previously described(*38*). Cell clustering was
704 computed with 30 principal components and resolution of 0.1. Marker genes were
705 identified by Wilcoxon Rank Sum test and log fold change of 0.25. Differential gene
706 expression analysis for selected genes (*COL1A1, COL1A2, CXCL12* and *IL6*) between
707 control and *HOTAIR* targeting GapmeR transfected SF were performed within each
708 SF cluster applying Wilcoxon Rank Sum test and FDR p-value adjustment for multiple
709 testing.

710 Table 3: Patient's characteristics (scRNAseq of control SF and SF silenced for
711 HOTAIR) (n=3)
712

Age (yrs)	72.7 ± 10.2
Female (n)	3
Osteoarthritis	3
Knee	3
CRP (mg/L)	1.0 ± 1.0
Treatnent	No

713

714

715

716 **In Situ Hybridization (ISH)**

717 *Construction of probes*

718 PCR on cDNA generated from total RNA of knee SF was used to produce an amplicon
719 of 267 base pairs of *HOTAIR* (see Table S4). Amplicons were cloned into pPCR-Script
720 Amp SK (+) plasmids using the PCR-Script Amp cloning kit (Agilent Technologies).
721 Plasmids were amplified and purified with the PureLink MiniPrep kit (Thermo Fisher
722 Scientific). Plasmids were linearized using restriction enzymes (EcoRI or NotI; both
723 New England Biolabs) and purified with the QIAquick PCR Purification Kit (Qiagen).
724 DIG-labeled *HOTAIR* probes were prepared by *in vitro* transcription with RNA
725 polymerases and plasmid vectors containing target transcript sequences. Linearized
726 plasmid DNA (10 µl) was used as a template, and RNA probes were synthesized with
727 T7 or T3 RNA polymerase (Roche) and DIG Labeling Mix (Roche) for 100 min at
728 37°C.

729 *In-situ hybridization*

730 *HOTAIR* expression was examined by ISH in paraffin-embedded synovial tissue from
731 OA and RA patients (for patients' characteristics see Table 2). All steps prior to and
732 during hybridization were conducted under RNase-free conditions. Sections were
733 deparaffinized, and incubated with HCl (20 min) and PFA 4% (10 min). Then sections
734 were treated with trypsin (1 mg/ml) at 37°C for 30 min. The slides were incubated
735 with 2X SSC 5 min and washed twice with triethanolamine-HCl solution. The sections
736 were acetylated for 20 min with 0.25% acetic anhydride in 0.1 M triethanolamine (pH
737 8.0) and washed twice in triethanolamine-HCl. Following incubation with
738 hybridization buffer for 1 h at RT, the sections were incubated with hybridization
739 solution which contained 1:10 diluted DIG-labelled probes in hybridization buffer
740 (50% deioned formamide, 40% dextran sulfate/SSC solution, 50x Denhardt's solution,

741 5% preheated herring sperm DNA and 250 µg/ml tRNA). Slides were then incubated
742 in a humidified chamber at 50°C overnight. After hybridization, slides were washed
743 with 5X SSC at 50°C (20 min), with 50% formamide in 2X SSC at 50°C (30 min) and
744 two times with STE buffer (500 mM NaCl, 1mM EDTA, 20mM TRIS-HCL pH 7.5).
745 Sections were treated with RNase A (40 µg/ml) in STE buffer at 37°C for 1 h, followed
746 by successive washing with STE buffer (RT), 2X SSC (RT), buffer 1 (0.2% SDS in
747 1X SSC, 50°C), buffer 2 (0.2% SDS in 0.5X SSC; 50°C)) and buffer 3 (0.2% SDS in
748 0.1X SSC; 50°C). Slides were incubated with 2% horse serum at RT for 30 min. Then
749 the slides were incubated in a humidified chamber at RT for 1 h with sheep anti-
750 digoxigenin-AP-Fab (Roche), diluted to 1:250 in TBS-T containing 1% blocking
751 reagent. Slides were washed with TBS-T and stained with nitro blue tetrazolium/5-
752 bromo-4-chloro-3-indolylphosphate (Roche) in the dark. The intensity of staining was
753 quantified with ImageJ software (http://rsbweb.nih.gov/ij/docs/examples/stained-
754 sections/index.html). Negative controls were conducted by the substitution of sense
755 for anti-sense probes or by the omission of anti-sense probes in the hybridization
756 solution.

757 **Immunohistochemistry**

758 For double staining of ISH slides, tissue sections were pre-treated with proteinase K
759 10 min at 37°C. Endogenous peroxidase activity was disrupted with 3% H_2O_2. Slides
760 were permeabilized with 0.1% Triton in PBS. Nonspecific protein binding was
761 blocked with 10% goat serum in antibody diluent (DakoCytomation) for 1 h. Mouse
762 anti-human CD68 (clone KP1; DakoCytomation) antibodies, mouse anti-human
763 vimentin (EPR3779; Abcam) antibodies or mouse IgG1 were applied over night at
764 4 °C. Slides were washed in PBS-T (0.05% Tween 20 in PBS) and incubated with

765 biotinylated goat anti-mouse antibodies (Jackson ImmunoResearch). The signal was
766 amplified with ABC reagent and detected with AEC (Vector laboratories).
767 Staining was imaged on a Zeiss Imager.Z1 (25x magnification) and quantified with
768 ImageJ using brightness values.

769 **Quantitative Real-time polymerase chain reaction (qPCR)**

770 Snap frozen synovial tissues were minced and total RNA was isolated using the
771 miRNeasy Mini kit (Qiagen) including on-column DNaseI digestion. From cultured
772 cells, total RNA was isolated using the Quick-RNA MicroPrep Kit (Zymo) including
773 on-column DNaseI digestion.
774 Total RNA was reversed transcribed and qPCR was performed using SYBR green
775 (Life Technologies) or TaqMan probes for the detection of *HOTAIR*. Primer sequences
776 are available in Tables S4 (human) and S5 (mouse). Changes after cycloheximide
777 adjunction (10ug/ml 6 h and 24 h) were evaluated (n = 3). No template control
778 samples, dissociation curves and samples containing the untranscribed RNA were
779 measured in parallel as controls. Data were analyzed with the comparative C_T method
780 and presented as ΔCT or $2^{-\Delta\Delta CT}$ as described(*68*). Constitutively expressed *HPRT* was
781 measured for internal standard sample normalization in humans and *beta2-*
782 *microglobulin* in mouse SF.

783 **SF stimulation**

784 SF were stimulated with human recombinant TNF (10 ng/ml; R&D Systems), human
785 recombinant IL1β (1 ng/ml; R&D Systems), lipopolysaccaride (LPS) from
786 *Escherichia coli* J5 (100 ng/ml; List Biological Laboratories), polyI-C (PIC) (10
787 µg/ml; InvivoGen), bacterial lipopeptide (bLP) palmitoyl-3-cysteine-serine-lysine-4

788 (300ng/ml; InvivoGen) or human recombinant TGFβ (10 ng/ml; R&D Systems) for
789 24 h.

790 **Cap Analysis Gene Expression (CAGE)**

791 CAGE data from control or TNF stimulated (10 ng/ml; 24 h) RA SF from 2 knees
792 were obtained from GSE163548. Mapping and identification of CAGE transcription
793 start sites (CTSSs) were performed by DNAFORM (Yokohama, Kanagawa, Japan).
794 In brief, the sequenced CAGE tags were mapped to hg19 using BWA software and
795 HISAT2 after discarding ribosomal RNAs. Identification of CTSSs was performed
796 with the Bioconductor package CAGEr (version 1.16.0)(*69*). Promoter and enhancer
797 candidate identification and quantification were performed with the Bioconductor
798 package CAGEfightR(*70*) (version 1.6.0) with default settings. Clusters were kept
799 when present in at least one sample.

800 **ChIP DNA sequencing**

801 SF pellets from OA knees transfected with GapmeR HOTAIR and GapmeR Control
802 (n = 3 each) were prepared using the iDeal ChIP seq kit for Histones (Diagenode) with
803 a shearing of 12 cycles (30″ON 30″OFF, Bioruptor Pico). The shearing efficiency was
804 analyzed using an automated capillary electrophoresis system Fragment Analyser
805 (High sensitivity NGS fragment kit) after RNase treatment, reversion of crosslinking
806 and purification of DNA. ChIP assays were performed using 1 million cells per IP and
807 H3K27me3 (1 µg, C15410195, Diagenode). A control library was processed in
808 parallel using the same amount of control Diagenode ChIP'd DNA. After the IP, the
809 ChIP'd DNA was analyzed by qPCR to evaluate the specificity of the reaction. The
810 promoter of GAPDH (GAPDH-TSS) was used as negative control region, Myelin
811 Transcription Factor 1 gene (MYT1) was used as a positive control region. The ratios

812 of the recovery for the positive regions over the background, i.e. the specificity of the
813 signal, were substantially smaller in two of the samples (one GapmeR HOTAIR and
814 one GapmeR control) (ratio MYT1/GAPDH-TSS 74 and 25, respectively compared
815 to a mean of 122 ±33 in the other samples). These samples also did not cluster with
816 the other samples in unsupervised principal component analysis. Therefore, these 2
817 samples were excluded for the analysis. Libraries were prepared from 1 ng of IP and
818 input DNA using the MicroPLEX v2 protocol, quantified by BioAnalyzer, purified
819 (AMPure beads) and eluted in TE. Purified libraries were quantified (Qubit ds DNA
820 HS kit), analysed for size (Fragment Analyzer) and diluted to 20 nM concentration.
821 Libraries were sequenced on an Illumina HiSeq 2500 (50 bp, single end).
822 The quality of sequencing reads was assessed using FastQC. Reads were aligned to
823 the reference genome (hg19) using BWA v. 0.7.5a(*71*). Samples were filtered for
824 regions blacklisted by the ENCODE project (*72, 73*). Subsequently samples were
825 deduplicated using SAMtools version 1.3.1(*74*). Alignment coordinates were
826 converted to BED format using BEDTools v.2.17(*74*). Peaks were annotated on gene
827 and transcript level using "ChIPpeakAnno", "ChIPQC", and "ChIPseeker" packages
828 of R. "DiffBind" package was used for differential binding.

829 **RNA sequencing**

830 Total RNA was isolated with the miRNeasy Mini kit (Qiagen) including on-column
831 DNaseI digestion from SF silenced for *HOTAIR* and control SF (n = 3 for each) 48 h
832 after the transfection. RNA quantity and quality were evaluated using the Agilent RNA
833 6000 Nano kit with the Agilent 2100 Bioanalyzer instrument (Agilent Technologies,
834 Inc.). The Illumina TruSeq Stranded total RNA protocol with the TruSeq Stranded
835 total RNA Sample Preparation Kit was used to produce RNA-seq libraries. The quality
836 and quantity of the generated libraries were determined by Agilent Technologies 2100

837 Bioanalyzer with DNA-specific chip and quantitative PCR (qPCR) using Illumina
838 adapter-specific primers using the Roche LightCycler system (Roche Diagnostics),
839 respectively. Diluted indexed long RNA-seq (10 nM) libraries were pooled in equal
840 volumes, used for cluster generation (TruSeq SR Cluster Kit v3-cBot-HS reagents,
841 according to the manufacturer's recommendations) and sequenced (TruSeq SBS Kit
842 v3-HS reagents, Illumina HiSeq4000). Sequencing data reads were quality-checked
843 with FastQC. Reads were trimmed with Trimmomatic and aligned to the reference
844 genome and transcriptome (FASTA and GTF files, respectively, Ensembl GRCh37)
845 with STAR(*75*). Gene expression was quantified using the R/Bioconductor package
846 Rsubread(*76*) version 1.22. Differentially expressed genes between conditions were
847 identified using the R/Bioconductor packages DESeq2(*77*).
848 Pathway enrichment analyses of genes differentially expressed between SF
849 invalidated for *HOTAIR* and controls were performed using Enrichr (all genes with
850 FDR < 0.05, log fold change +/-1)(*65*). The scatter dot plot was created with the
851 Enrichr Appyter.

852 **ELISA**

853 The human CXCL12 DuoSet ELISA kit (R&D Systems), the human IL12-p35 ELISA
854 kit (Elabscience), the human IL6 ELISA DuoSet kit (R&D Systems), and the human
855 procollagen 1α ELISA Set (BD Biosciences), respectively was used with cell culture
856 supernatants.

857 **SF organ micromasses**

858 3D micromasses were generated as previously described(*78*). In brief, SF transfected
859 with control or *HOTAIR* GapmeR were mixed with Matrigel (LDEV-free, Corning)
860 ($3x10^6$ SF/ml Matrigel) and 30 µl droplets added to 12-well plates coated with poly 2-

861 hydroxyethylmethacrylate (Sigma). Micromasses were left in culture for 3 weeks in
862 Dulbecco's modified Eagle's medium (DMEM; Life Technologies) supplemented
863 with 10% fetal calf serum (FCS), 1% penicillin/streptomycin, 1% minimum Essential
864 medium non-Essential Amino Acids (Giboc), 1% ITS + premix (BD) und 17.6 µg/ml
865 vitamin C. After 3 weeks, micromasses were fixed with 2% paraformaldehyde. After
866 24 h, paraformaldehyde was replaced by 70% ethanol and micromasses were
867 embedded in paraffin and sectioned for IHC. Spheroids were stained with anti-human
868 collagen I antibodies (EPR7785, Abcam) on a BOND-MAX autostainer (Leica).
869 Staining was imaged on a Zeiss Imager.Z1 (25x magnification) and quantified with
870 ImageJ using brightness values.

871 **Western blotting**

872 Cells were lysed in Laemmli buffer (62.5 mM TrisHCl, 2% SDS, 10% Glycerol, 0.1%
873 Bromphenolblue, 5 mM β-mercaptoethanol). Whole cell lysates were separated on
874 10% SDS polyacrylamide gels and electroblotted onto nitrocellulose membranes
875 (Whatman). Membranes were blocked for 1 h in 5% (w/v) non-fat milk in TBS-T (20
876 mM Tris base, 137 mM sodium chloride, 0.1% Tween-20, pH 7.6) or in 5% (w/v)
877 BSA in TBS-T BSA for phosphorylated proteins. After blocking, the membranes were
878 probed with antibodies against p-AKT (4060, Cell Signaling), AKT (4685, Cell
879 Signaling) α-tubulin (ab7291, abcam) overnight at 4°C. As secondary antibodies,
880 horseradish peroxidase-conjugated goat anti-rabbit (111-036-047, Jackson
881 ImmunoResearch) or goat anti-mouse antibodies (115-036-062, Jackson
882 ImmunoResearch) were used. Signals were detected using the ECL Western blotting
883 detection reagents (GE Healthcare) and the Alpha Imager Software system (Alpha
884 Innotech).

885 **Luciferase activity assay**

886 To measure the effect of HOTAIR silencing on the canonical Wnt pathway, SF were
887 transfected by electroporation (BTX) with the beta-catenin reporter M50 Super 8x
888 TOPFlash (Addgene plasmid #12456) or M51 Super 8x FOPFlash, which contains
889 mutated binding sites upstream of the luciferase reporter (Addgene plasmid
890 #12457)(*79*). Both plasmids were a gift from Randall Moon. For normalization,
891 pRenilla Luciferase Control Reporter Vectors (Promega) were co-transfected. 24 h
892 after transfection, cells were transfected with GapmeR for *HOTAIR* or control as
893 mentioned above. Luciferase activity was measured with a dual luciferase reporter
894 assay system (Promega), and the results were normalized to the activity of Renilla
895 luciferase.

896 **Real-time cell analysis (RTCA)**

897 For RTCA of cell adhesion and proliferation of SF, the xCELLigence RTCA DP
898 Instrument (ACEA Biosciences, Inc.) was used. 16-well E-plates were equilibrated
899 with 100 µl of DMEM, 10% FCS for 30 min at RT. The impedance, expressed as
900 arbitrary Cell Index (CI) units, of the wells with media alone (background impedance–
901 Rb) was measured before adding the cells. SF were detached with accutase (Merck),
902 resuspended in DMEM, and seeded at a cell density of 25,000 cells per well. Cell
903 adhesion and spreading, measured as changes in impedance, was monitored every
904 5 min for a period of first 12 h and every 15 min after that for the next 12 h. The CI at
905 each time point is defined as (Rn−Rb)/15, where Rn is the cell-electrode impedance
906 of the well when it contains cells and Rb is the background impedance. Each condition
907 was analysed in quadruplicates. Impedance changes were recorded every 15 min (0–
908 24 h) and every 30 min (24–245 h). Adhesion was analysed over the first 16 h of the

909 experiment, spreading was analysed between 17 and 127 h and proliferation during
910 the exponential phase of the slopes (120-245).

911 **Scratch assay**

912 To assess real time migration of SF, we performed a scratch assay(*80*) using Ibidi
913 culture inserts (Ibidi, Germany) with 70 µl cell suspension (1.2×10^5 cells/ml). Cells
914 were incubated at 37 °C and 5% CO_2 for 24 h to obtain a confluent cell layer. Next,
915 cells were transfected with GapmeR *HOTAIR* or controls and incubated for additional
916 24 h. Culture inserts were removed and cell layers were washed with PBS. Culture
917 medium (with vitamin C) was added and time lapse images were recorded every 30
918 minutes for 48 hours using a widefield Zeiss AxioObserver equipped with a stage
919 incubator to maintain temperature and CO_2 conditions. Each assay was performed in
920 triplicate and repeated three times. Open area was calculated over 24 h to 48 h
921 according to experiments(*80*).

922 **Apoptosis assay**

923 Activity of the key effector caspases 3 and 7 was measured using the Caspase-Glo 3/7
924 assay (Promega, Madison, WI). SF were seeded at a density of 4000 cells/well in 96-
925 well white-walled plates. The next day, SF were transfected with GapmeR for
926 *HOTAIR* or GapmeR control or left untransfected. Cleaved caspase 3/7 activity was
927 assessed 48 h after transfection. FAS-ligand (2 µg/ml) was added 18 h before the assay
928 to stimulate apoptosis. Luminescence signals were measured using a Synergy HT
929 microplate reader (Bio Tek). Each assay was performed in triplicate and repeated two
930 times.

931 **Osteoclastogenesis assay**

932 Human osteoclasts precursors were isolated from blood donations of healthy
933 volunteers (*n* = 4, Red Cross, Schlieren, Switzerland). In brief, CD14+ cells were
934 isolated by positive selection using magnetic separation (Milteny Biotec) after a Ficoll
935 gradient (GE Healthcare) separation. Isolated monocytes (5 x 10^4) were cultured in
936 chamber slides in αMEM supplemented with 10% FBS (GE Healthcare), 2 mM l-
937 glutamine and antibiotics in the presence of 25 ng/mL macrophage colony-stimulating
938 factor (M-CSF) (PeproTech) for 3 days. SF were transfected with *HOTAIR* or control
939 GapmeR and were added to differentiating monocytes (5 x 10^5 SF/well). Alternatively,
940 supernatants from control or *HOTAIR* silenced SF were added. Cells were cultured in
941 the presence of 25 ng/mL M-CSF, 50 ng/mL RANKL (PeproTech) and vitamin C. The
942 media was replaced every 2 days. After 6 days of culture, the cells were fixed by 4%
943 paraformaldehyde and were stained by TRAP. Control experiments included
944 untransfected SF, SF alone (without precursors of osteoclasts) and precursors without
945 SF or supernatants. Each assay was performed in duplicate and repeated three times.
946 To assess bone resorption, osteoclasts precursors (10^5/well) were co-cultured with SF
947 (1.5 x 10^4/well) or supernatants from SF in 96 wells on bovine bone slices (Jelling,
948 Denmark) for two weeks in the presence of 25 ng/mL M-CSF, 50 ng/mL RANKL and
949 vitamin C. The osteoclastogenic medium was replaced every 2–3 days. SF were re-
950 transfected every 5 days with *HOTAIR* or control GapmeRs. Analyses were done after
951 14 days of differentiation. Cells on bone slices were subsequently incubated with a 0.1
952 m NaOH solution, ultrasonicated for 2 min, rinsed with water to remove cells from the
953 slices, and placed in a 1% aqueous toluidine blue solution containing 1% sodium
954 borate for 5 min. Photomicrographs of resorption pits were taken using a light
955 microscope. Resorption area was measured using Image J.

956 **Chemotaxis assay**

957 PBMCs from one healthy donor were isolated using CPT™ tubes (BD Biosciences)
958 and 10^6 PBMCs were seeded in the upper well of a 96-well transwell migration
959 chamber with 5 µm pore size (Corning). The lower chamber was filled with
960 supernatants collected from control or *HOTAIR* silenced SF 48h after transfection
961 (triplicates). Unconditioned medium or PBS were used as controls. Cells were
962 collected from the lower chamber after 18h using ice-cold 20mM EDTA/0.5% FCS in
963 PBS as detachment solution. Collected cells were counted in a cell counter (Casy,
964 OLS) and stained with anti-human CD14-PE, anti-human CD19-PE or anti-human
965 CD3-FITC antibodies (all Miltenyi) for 1 h at 4°C. FITC- and PE-labelled IgG were
966 used as negative control antibodies. Percentage of positive cells was assessed on a
967 FACSCalibur™ flow cytometry platform (BD Biosciences).

968 **RNA sequencing from the early arthritis cohort**

969 RNA-sequencing data from the Pathobiology of Early Arthritis Cohort, which is
970 available on the PEAC (qmul.ac.uk) was studied.

971 **Isolation of mouse tissue from lung, spine and gut**

972 Wild-type C57BL/6 mice, 6 weeks old, were purchased from Jackson and dissected.
973 The spine and gut were isolated and separated into different parts (spine: cervical,
974 thoracic and lumbal) and gut (stomach, small intestine, caecum, colon and rectum).
975 Total RNA was isolated using the miRNeasy Mini kit (Qiagen) including on-column
976 DNaseI digestion. Total RNA was reversed transcribed and qPCR was performed
977 using SYBR green (Life Technologies). Constitutively expressed *beta2-microglobulin*
978 was measured for internal standard sample normalization. In cases of undetectable
979 expression of *Hotair* in mouse tissue*s* the ct was set arbitrarily to 45 in order to
980 calculate the dct.

981 **Statistical analysis**

982 Data were analysed with GraphPad Prism version 6.0 or higher and IBM SPSS
983 Statistics software. Two groups were compared with two-tailed unpaired or paired t
984 test, as appropriate. Multiple group comparisons were performed by adjustments for
985 multiple comparisons using Bonferroni correction or two-way ANOVA. Correlations
986 were tested using Spearman's correlation coefficient. P values of <0.05 were
987 considered statistically significant.

988 **Study approval**

989 The collection and experimental usage of the human samples was approved by the
990 ethical commission of the Kanton Zurich (swissethics number: 2019-00674, PB-2016-
991 02014 and 2019-00115). Informed consent was obtained from all patients. All
992 experiments have been performed in accordance with the institutional guidelines.
993 Mouse experiments were approved by the Institutional Committee of Protocol
994 Evaluation in conjunction with the Veterinary Service Management of the Hellenic
995 Republic Prefecture of Attika according to all current European and national
996 legislation and were performed in accordance with relevant guidelines and regulations,
997 under the relevant animal protocol licenses with number 2199-11/4/2017.

998 **Data availability**

999 The RNA seq, ChIP seq of H3K27me3 and the scRNA seq data with control GapmeR
1000 and *HOTAIR* GapmeR transfected SF are uploaded to the GEO repository accession
1001 GSE185440.

1002

1003

1004

1005 **AUTHOR CONTRIBUTIONS**

1006 CO, ME and RM designed, analyzed and interpreted experiments. ME, CO, RM and MH
1007 wrote the manuscript. ME, MH, MaMi, LM, CP, KB, KK, PS, MFB and SGE performed
1008 experiments. RM and MH did the computational analysis. ME, AL, GK, MS, GeKo, MA
1009 and CO performed the mouse experiments. RM, KB and OD organized ethic approval,
1010 recruited patients and collected samples. All authors critically reviewed the manuscript.

1011

1012 **ACKNOWLEDGMENTS**

1013 We thank Maria Comazzi and Peter Künzler (Center of Experimental Rheumatology,
1014 University Hospital Zurich, Switzerland) for excellent technical assistance. We thank
1015 Miriam Marks for providing the samples from joint replacement.
1016 ME was supported by Société Française de Rhumatologie, Fondation pour la
1017 Recherche Médicale, Assistance publique - Hôpitaux de Paris (APHP) and EULAR.
1018 CO was supported by the Hartmann-Müller Foundation, the Foundation for Research
1019 in Science and the Humanities at the University of Zurich, the EMDO Foundation and
1020 the Iten-Kohaut Foundation. This work was supported by the IMI project BTCure (GA
1021 no. 115142-2). We also acknowledge support by the InfrafrontierGR infrastructure
1022 (MIS 5002135), co-funded by Greece and the European Union [European Regional
1023 Development Fund] under NSRF 2014–2020, which provided mouse hosting and
1024 phenotyping facilities. The graphical abstract was created with BioRender.com.

1025 **CONFLICTS OF INTEREST**

1026 Muriel Elhai, Raphael Micheroli, Miranda Houtman, Masoumeh Mirrahimi, Larissa
1027 Moser, Chantal Pauli, Kristina Bürki, Andrea Laimbacher, Gabriela Kania, Kerstin
1028 Klein, Philipp Schätzle, Mojca Frank Bertoncelj, Sam G. Edalat, Maria Sakkou,
1029 George Kollias, Marietta Armaka, and Caroline Ospelt: none

Oliver Distler has/had relationships with the following companies in the area of potential treatments for systemic sclerosis and its complications in the last three calendar years:

Speaker fee: Bayer, Boehringer Ingelheim, Janssen, Medscape

Consultancy fee: 4P-Pharma, Abbvie, Acceleron, Alcimed, Altavant Siences, Amgen, AnaMar, Arxx, AstraZeneca, Baecon, Blade, Bayer, Boehringer Ingelheim, Corbus, CSL Behring, Galapagos, Glenmark, Horizon, Inventiva, Kymera, Lupin, Miltenyi Biotec, Mitsubishi Tanabe, MSD, Novartis, Prometheus, Redxpharna, Roivant, Sanofi and Topadur

Research Grants: Kymera, Mitsubishi Tanabe, Boehringer Ingelheim

Oliver Distler has/had relationships with the following companies in the area of potential treatments for dermatomyositis and its complications in the last three calendar years:

Consultancy fee for rheumatology topic: Pfizer (2021)

Oliver Distler has/had relationships with the following companies in the area of potential treatments for arthritides in the last three

Consultancy fee: Abbvie

REFERENCES

1. Global, regional, and national incidence, prevalence, and years lived with disability for 354 diseases and injuries for 195 countries and territories, 1990-2017: a systematic analysis for the Global Burden of Disease Study 2017. *Lancet* **392**, 1789-1858 (2018).
2. J. W. J. Bijlsma, E. Hachulla, J. A. P. da Silva, M. Doherty, J. M. van Laar, M. A. Cimmino, F. Lioté, *EULAR textbook on rheumatic diseases* (BMJ Publishing Group United Kingdom, 2018).
3. D. van der Woude, A. H. M. van der Helm-van Mil, Update on the epidemiology, risk factors, and disease outcomes of rheumatoid arthritis. *Best practice & research. Clinical rheumatology* **32**, 174-187 (2018).
4. M. H. Buch, S. Eyre, D. McGonagle, Persistent inflammatory and non-inflammatory mechanisms in refractory rheumatoid arthritis. *Nat Rev Rheumatol* **17**, 17-33 (2021).
5. A. Ciurea, O. Distler, T. Killeen, E. Akylbekova, K. Kwok, L. Wang, C. Ospelt, M. Frank-Bertoncelj, FRI0144 JOINT-SPECIFIC RESPONSES TO TOFACITINIB AND ADALIMUMAB IN RHEUMATOID ARTHRITIS: A POST HOC ANALYSIS OF DATA FROM ORAL STANDARD AND ORAL STRATEGY. *Annals of the Rheumatic Diseases* **78**, 742-743 (2019).
6. G. Dennis, Jr., C. T. Holweg, S. K. Kummerfeld, D. F. Choy, A. F. Setiadi, J. A. Hackney, P. M. Haverty, H. Gilbert, W. Y. Lin, L. Diehl, S. Fischer, A. Song, D. Musselman, M. Klearman, C. Gabay, A. Kavanaugh, J. Endres, D. A. Fox, F. Martin, M. J. Townsend, Synovial phenotypes in rheumatoid arthritis correlate with response to biologic therapeutics. *Arthritis Res Ther* **16**, R90 (2014).
7. T. C. van der Pouw Kraan, F. A. van Gaalen, T. W. Huizinga, E. Pieterman, F. C. Breedveld, C. L. Verweij, Discovery of distinctive gene expression profiles in rheumatoid synovium using cDNA microarray technology: evidence for the existence of multiple pathways of tissue destruction and repair. *Genes Immun* **4**, 187-196 (2003).
8. D. E. Orange, P. Agius, E. F. DiCarlo, N. Robine, H. Geiger, J. Szymonifka, M. McNamara, R. Cummings, K. M. Andersen, S. Mirza, M. Figgie, L. B. Ivashkiv, A. B. Pernis, C. S. Jiang, M. O. Frank, R. B. Darnell, N. Lingampali, W. H. Robinson, E. Gravallese, V. P. Bykerk, S. M. Goodman, L. T. Donlin, Identification of Three Rheumatoid Arthritis Disease Subtypes by Machine Learning Integration of Synovial Histologic Features and RNA Sequencing Data. *Arthritis Rheumatol* **70**, 690-701 (2018).
9. F. Humby, M. Lewis, N. Ramamoorthi, J. A. Hackney, M. R. Barnes, M. Bombardieri, A. F. Setiadi, S. Kelly, F. Bene, M. DiCicco, S. Riahi, V. Rocher, N. Ng, I. Lazarou, R. Hands, D. van der Heijde, R. B. M. Landewé, A. van der Helm-van Mil, A. Cauli, I. McInnes, C. D. Buckley, E. H. Choy, P. C. Taylor, M. J. Townsend, C. Pitzalis, Synovial cellular and molecular signatures stratify clinical response to csDMARD therapy and predict radiographic progression in early rheumatoid arthritis patients. *Ann Rheum Dis* **78**, 761-772 (2019).
10. F. Rivellese, A. E. A. Surace, K. Goldmann, E. Sciacca, C. Çubuk, G. Giorli, C. R. John, A. Nerviani, L. Fossati-Jimack, G. Thorborn, M. Ahmed, E. Prediletto, S. E. Church, B. M. Hudson, S. E. Warren, P. M. McKeigue, F. Humby, M. Bombardieri, M. R. Barnes, M. J. Lewis, C. Pitzalis, Rituximab versus tocilizumab in rheumatoid arthritis: synovial biopsy-based biomarker analysis of the phase 4 R4RA randomized trial. *Nat Med* **28**, 1256-1268 (2022).
11. R. Patel, A. Filer, F. Barone, C. D. Buckley, Stroma: fertile soil for inflammation. *Best Pract Res Clin Rheumatol* **28**, 565-576 (2014).
12. M. Frank-Bertoncelj, S. Gay, The epigenome of synovial fibroblasts: an underestimated therapeutic target in rheumatoid arthritis. *Arthritis Res Ther* **16**, 117 (2014).
13. F. Zhang, K. Wei, K. Slowikowski, C. Y. Fonseka, D. A. Rao, S. Kelly, S. M. Goodman, D. Tabechian, L. B. Hughes, K. Salomon-Escoto, G. F. M. Watts, A. H. Jonsson, J. Rangel-Moreno, N. Meednu, C. Rozo, W. Apruzzese, T. M. Eisenhaure, D. J. Lieb, D. L. Boyle, A. M. Mandelin, 2nd, B. F. Boyce, E. DiCarlo, E. M. Gravallese, P. K. Gregersen, L. Moreland, G. S. Firestein, N. Hacohen, C. Nusbaum, J. A. Lederer, H. Perlman, C. Pitzalis, A. Filer, V. M. Holers, V. P. Bykerk, L. T. Donlin, J. H. Anolik, M. B. Brenner, S. Raychaudhuri, Defining inflammatory cell states in rheumatoid arthritis joint synovial tissues by integrating single-cell transcriptomics and mass cytometry. *Nat Immunol* **20**, 928-942 (2019).
14. K. Wei, I. Korsunsky, J. L. Marshall, A. Gao, G. F. M. Watts, T. Major, A. P. Croft, J. Watts, P. E. Blazar, J. K. Lange, T. S. Thornhill, A. Filer, K. Raza, L. T. Donlin, C. W. Siebel, C. D.

Buckley, S. Raychaudhuri, M. B. Brenner, Notch signalling drives synovial fibroblast identity and arthritis pathology. *Nature* **582**, 259-264 (2020).

15. F. Mizoguchi, K. Slowikowski, K. Wei, J. L. Marshall, D. A. Rao, S. K. Chang, H. N. Nguyen, E. H. Noss, J. D. Turner, B. E. Earp, P. E. Blazar, J. Wright, B. P. Simmons, L. T. Donlin, G. D. Kalliolias, S. M. Goodman, V. P. Bykerk, L. B. Ivashkiv, J. A. Lederer, N. Hacohen, P. A. Nigrovic, A. Filer, C. D. Buckley, S. Raychaudhuri, M. B. Brenner, Functionally distinct disease-associated fibroblast subsets in rheumatoid arthritis. *Nat Commun* **9**, 789 (2018).
16. A. P. Croft, J. Campos, K. Jansen, J. D. Turner, J. Marshall, M. Attar, L. Savary, C. Wehmeyer, A. J. Naylor, S. Kemble, J. Begum, K. Dürholz, H. Perlman, F. Barone, H. M. McGettrick, D. T. Fearon, K. Wei, S. Raychaudhuri, I. Korsunsky, M. B. Brenner, M. Coles, S. N. Sansom, A. Filer, C. D. Buckley, Distinct fibroblast subsets drive inflammation and damage in arthritis. *Nature* **570**, 246-251 (2019).
17. M. Frank-Bertoncelj, M. Trenkmann, K. Klein, E. Karouzakis, H. Rehrauer, A. Bratus, C. Kolling, M. Armaka, A. Filer, B. A. Michel, R. E. Gay, C. D. Buckley, G. Kollias, S. Gay, C. Ospelt, Epigenetically-driven anatomical diversity of synovial fibroblasts guides joint-specific fibroblast functions. *Nat Commun* **8**, 14852 (2017).
18. J. L. Rinn, M. Kertesz, J. K. Wang, S. L. Squazzo, X. Xu, S. A. Brugmann, L. H. Goodnough, J. A. Helms, P. J. Farnham, E. Segal, H. Y. Chang, Functional demarcation of active and silent chromatin domains in human HOX loci by noncoding RNAs. *Cell* **129**, 1311-1323 (2007).
19. M. C. Tsai, O. Manor, Y. Wan, N. Mosammaparast, J. K. Wang, F. Lan, Y. Shi, E. Segal, H. Y. Chang, Long noncoding RNA as modular scaffold of histone modification complexes. *Science* **329**, 689-693 (2010).
20. Y. Yokouchi, H. Sasaki, A. Kuroiwa, Homeobox gene expression correlated with the bifurcation process of limb cartilage development. *Nature* **353**, 443-445 (1991).
21. S. Yamamoto, Y. Uchida, T. Ohtani, E. Nozaki, C. Yin, Y. Gotoh, N. Yakushiji-Kaminatsui, T. Higashiyama, T. Suzuki, T. Takemoto, Y. I. Shiraishi, A. Kuroiwa, Hoxa13 regulates expression of common Hox target genes involved in cartilage development to coordinate the expansion of the autopodal anlage. *Dev Growth Differ* **61**, 228-251 (2019).
22. R. P. Visconti, A. Awgulewitsch, Topographic patterns of vascular disease: HOX proteins as determining factors? *World J Biol Chem* **6**, 65-70 (2015).
23. N. Yahagi, R. Kosaki, T. Ito, T. Mitsuhashi, H. Shimada, M. Tomita, T. Takahashi, K. Kosaki, Position-specific expression of Hox genes along the gastrointestinal tract. *Congenit Anom (Kyoto)* **44**, 18-26 (2004).
24. F. C. Kuo, M. J. Neville, R. Sabaratnam, A. Wesolowska-Andersen, D. Phillips, L. B. L. Wittemans, A. D. van Dam, N. Y. Loh, M. Todorčević, N. Denton, K. A. Kentistou, P. K. Joshi, C. Christodoulides, C. Langenberg, P. Collas, F. Karpe, K. E. Pinnick, HOTAIR interacts with PRC2 complex regulating the regional preadipocyte transcriptome and human fat distribution. *Cell Rep* **40**, 111136 (2022).
25. V. Krenn, L. Morawietz, G. R. Burmester, R. W. Kinne, U. Mueller-Ladner, B. Muller, T. Haupl, Synovitis score: discrimination between chronic low-grade and high-grade synovitis. *Histopathology* **49**, 358-364 (2006).
26. I. B. McInnes, G. Schett, Pathogenetic insights from the treatment of rheumatoid arthritis. *Lancet* **389**, 2328-2337 (2017).
27. T. Seitz, C. Hellerbrand, Role of fibroblast growth factor signalling in hepatic fibrosis. *Liver Int* **41**, 1201-1215 (2021).
28. D. ten Berge, S. A. Brugmann, J. A. Helms, R. Nusse, Wnt and FGF signals interact to coordinate growth with cell fate specification during limb development. *Development* **135**, 3247-3257 (2008).
29. C. M. Teven, E. M. Farina, J. Rivas, R. R. Reid, Fibroblast growth factor (FGF) signaling in development and skeletal diseases. *Genes Dis* **1**, 199-213 (2014).
30. W. Kim, S. Min, M. Cho, J. Youn, J. Min, S. Lee, S. Park, C. Cho, H. Kim, The role of IL-12 in inflammatory activity of patients with rheumatoid arthritis (RA). *Clinical and experimental immunology* **119**, 175-181 (2000).
31. R. Bucala, C. Ritchlin, R. Winchester, A. Cerami, Constitutive production of inflammatory and mitogenic cytokines by rheumatoid synovial fibroblasts. *The Journal of experimental medicine* **173**, 569-574 (1991).
32. T. Nanki, K. Hayashida, H. S. El-Gabalawy, S. Suson, K. Shi, H. J. Girschick, S. Yavuz, P. E. Lipsky, Stromal cell-derived factor-1-CXC chemokine receptor 4 interactions play a central role in CD4+ T cell accumulation in rheumatoid arthritis synovium. *J Immunol* **165**, 6590-6598 (2000).

33. T. Pap, J. K. Franz, K. M. Hummel, E. Jeisy, R. Gay, S. Gay, Activation of synovial fibroblasts in rheumatoid arthritis: lack of Expression of the tumour suppressor PTEN at sites of invasive growth and destruction. *Arthritis research* **2**, 59-64 (2000).
34. A. M. Grabiec, C. Angiolilli, L. M. Hartkamp, L. G. van Baarsen, P. P. Tak, K. A. Reedquist, JNK-dependent downregulation of FoxO1 is required to promote the survival of fibroblast-like synoviocytes in rheumatoid arthritis. *Ann Rheum Dis* **74**, 1763-1771 (2015).
35. M. Armaka, D. Konstantopoulos, C. Tzaferis, M. D. Lavigne, M. Sakkou, A. Liakos, P. P. Sfikakis, M. A. Dimopoulos, M. Fousteri, G. Kollias, Single-cell multimodal analysis identifies common regulatory programs in synovial fibroblasts of rheumatoid arthritis patients and modeled TNF-driven arthritis. *Genome Med* **14**, 78 (2022).
36. F. Zhang, K. Wei, K. Slowikowski, C. Y. Fonseka, D. A. Rao, S. Kelly, S. M. Goodman, D. Tabechian, L. B. Hughes, K. Salomon-Escoto, G. F. M. Watts, A. H. Jonsson, J. Rangel-Moreno, N. Meednu, C. Rozo, W. Apruzzese, T. M. Eisenhaure, D. J. Lieb, D. L. Boyle, A. M. Mandelin, 2nd, A. Accelerating Medicines Partnership Rheumatoid, C. Systemic Lupus Erythematosus, B. F. Boyce, E. DiCarlo, E. M. Gravallese, P. K. Gregersen, L. Moreland, G. S. Firestein, N. Hacohen, C. Nusbaum, J. A. Lederer, H. Perlman, C. Pitzalis, A. Filer, V. M. Holers, V. P. Bykerk, L. T. Donlin, J. H. Anolik, M. B. Brenner, S. Raychaudhuri, Defining inflammatory cell states in rheumatoid arthritis joint synovial tissues by integrating single-cell transcriptomics and mass cytometry. *Nature immunology* **20**, 928-942 (2019).
37. W. Stephenson, L. T. Donlin, A. Butler, C. Rozo, B. Bracken, A. Rashidfarrokhi, S. M. Goodman, L. B. Ivashkiv, V. P. Bykerk, D. E. Orange, R. B. Darnell, H. P. Swerdlow, R. Satija, Single-cell RNA-seq of rheumatoid arthritis synovial tissue using low-cost microfluidic instrumentation. *Nat Commun* **9**, 791 (2018).
38. R. Micheroli, M. Elhai, S. Edalat, M. Frank-Bertoncelj, K. Burki, A. Ciurea, L. MacDonald, M. Kurowska-Stolarska, M. J. Lewis, K. Goldmann, C. Cubuk, T. Kuret, O. Distler, C. Pitzalis, C. Ospelt, Role of synovial fibroblast subsets across synovial pathotypes in rheumatoid arthritis: a deconvolution analysis. *RMD Open* **8**, (2022).
39. C. Li, C. Fei, J. Li, H. Wu, L. Chen, R. Roshani, H. Li, L. Shi, C. Song, J. Gu, Y. Lu, Q. Zhou, SMARCC2 combined with c-Myc inhibits the migration and invasion of glioma cells via modulation of the Wnt/β-catenin signaling pathway. *Molecular medicine reports* **24**, (2021).
40. C. G. Miao, Y. Y. Yang, X. He, X. F. Li, C. Huang, Y. Huang, L. Zhang, X. W. Lv, Y. Jin, J. Li, Wnt signaling pathway in rheumatoid arthritis, with special emphasis on the different roles in synovial inflammation and bone remodeling. *Cellular signalling* **25**, 2069-2078 (2013).
41. F. Grassi, S. Cristino, S. Toneguzzi, A. Piacentini, A. Facchini, G. Lisignoli, CXCL12 chemokine up-regulates bone resorption and MMP-9 release by human osteoclasts: CXCL12 levels are increased in synovial and bone tissue of rheumatoid arthritis patients. *Journal of cellular physiology* **199**, 244-251 (2004).
42. G. Lliso-Ribera, F. Humby, M. Lewis, A. Nerviani, D. Mauro, F. Rivellese, S. Kelly, R. Hands, F. Bene, N. Ramamoorthi, J. A. Hackney, A. Cauli, E. H. Choy, A. Filer, P. C. Taylor, I. McInnes, M. J. Townsend, C. Pitzalis, Synovial tissue signatures enhance clinical classification and prognostic/treatment response algorithms in early inflammatory arthritis and predict requirement for subsequent biological therapy: results from the pathobiology of early arthritis cohort (PEAC). *Ann Rheum Dis* **78**, 1642-1652 (2019).
43. A. Bhan, P. Deb, N. Shihabeddin, K. I. Ansari, M. Brotto, S. S. Mandal, Histone methylase MLL1 coordinates with HIF and regulate lncRNA HOTAIR expression under hypoxia. *Gene* **629**, 16-28 (2017).
44. H. Qiu, M. Liu, X. Shi, M. Ma, J. Zhang, H. Liu, LncRNA HOTAIR inhibits the progression of fibroblast-like synoviocytes by sponging miRNA-106b-5p in rheumatoid arthritis. *Autoimmunity* **55**, 567-576 (2022).
45. K. Carrion, J. Dyo, V. Patel, R. Sasik, S. A. Mohamed, G. Hardiman, V. Nigam, The long non-coding HOTAIR is modulated by cyclic stretch and WNT/β-CATENIN in human aortic valve cells and is a novel repressor of calcification genes. *PLoS One* **9**, e96577 (2014).
46. C. Cheng, Y. Qin, Q. Zhi, J. Wang, C. Qin, Knockdown of long non-coding RNA HOTAIR inhibits cisplatin resistance of gastric cancer cells through inhibiting the PI3K/Akt and Wnt/β-catenin signaling pathways by up-regulating miR-34a. *International journal of biological macromolecules* **107**, 2620-2629 (2018).
47. Y. Tang, G. Song, H. Liu, S. Yang, X. Yu, L. Shi, Silencing of Long Non-Coding RNA HOTAIR Alleviates Epithelial-Mesenchymal Transition in Pancreatic Cancer via the Wnt/β-Catenin Signaling Pathway. *Cancer management and research* **13**, 3247-3257 (2021).

48. J. Hu, Z. Wang, Y. Shan, Y. Pan, J. Ma, L. Jia, Long non-coding RNA HOTAIR promotes osteoarthritis progression via miR-17-5p/FUT2/β-catenin axis. *Cell death & disease* **9**, 711 (2018).
49. Y. Yang, D. Xing, Y. Wang, H. Jia, B. Li, J. J. Li, A long non-coding RNA, HOTAIR, promotes cartilage degradation in osteoarthritis by inhibiting WIF-1 expression and activating Wnt pathway. *BMC Mol Cell Biol* **21**, 53 (2020).
50. X. H. Meng, Z. Wang, X. N. Zhang, J. Xu, Y. C. Hu, Rheumatoid Arthritis of Knee Joints: MRI-Pathological Correlation. *Orthop Surg* **10**, 247-254 (2018).
51. L. Punzi, R. Ramonda, P. Sfriso, Erosive osteoarthritis. *Best practice & research* **18**, 739-758 (2004).
52. J. Lu, Z. Wu, Y. Xiong, Knockdown of long noncoding RNA HOTAIR inhibits osteoarthritis chondrocyte injury by miR-107/CXCL12 axis. *J Orthop Surg Res* **16**, 410 (2021).
53. A. R. Amândio, A. Necsulea, E. Joye, B. Mascrez, D. Duboule, Hotair Is Dispensible for Mouse Development. *PLoS Genet* **12**, e1006232 (2016).
54. X. Hu, J. P. Charles, T. Akay, J. R. Hutchinson, S. S. Blemker, Are mice good models for human neuromuscular disease? Comparing muscle excursions in walking between mice and humans. *Skelet Muscle* **7**, 26 (2017).
55. D. Xu, L. Sun, HOTAIR underlies the region-specific development of adipose tissue. *Nat Rev Endocrinol* **18**, 663-664 (2022).
56. S. Brophy, K. Mackay, A. Al-Saidi, G. Taylor, A. Calin, The natural history of ankylosing spondylitis as defined by radiological progression. *J Rheumatol* **29**, 1236-1243 (2002).
57. A. van Tubergen, D. van der Heijde, M. Dougados, H. Mielants, R. Landewé, Are syndesmophytes most prevalent in the lumbar or in the cervical spine in patients with ankylosing spondylitis and do they develop in a specific direction? *Rheumatology (Oxford)* **51**, 1432-1439 (2012).
58. D. Wendling, P. Claudepierre, New bone formation in axial spondyloarthritis. *Joint Bone Spine* **80**, 454-458 (2013).
59. C. McDowell, U. Farooq, M. Haseeb, "Inflammatory Bowel Disease" in *StatPearls* (StatPearls Publishing
Copyright © 2022, StatPearls Publishing LLC., Treasure Island (FL), 2022).
60. L. Moparthi, S. Koch, Wnt signaling in intestinal inflammation. *Differentiation* **108**, 24-32 (2019).
61. D. Aletaha, T. Neogi, A. J. Silman, J. Funovits, D. T. Felson, C. O. Bingham, 3rd, N. S. Birnbaum, G. R. Burmester, V. P. Bykerk, M. D. Cohen, B. Combe, K. H. Costenbader, M. Dougados, P. Emery, G. Ferraccioli, J. M. Hazes, K. Hobbs, T. W. Huizinga, A. Kavanaugh, J. Kay, T. K. Kvien, T. Laing, P. Mease, H. A. Ménard, L. W. Moreland, R. L. Naden, T. Pincus, J. S. Smolen, E. Stanislawska-Biernat, D. Symmons, P. P. Tak, K. S. Upchurch, J. Vencovský, F. Wolfe, G. Hawker, 2010 Rheumatoid arthritis classification criteria: an American College of Rheumatology/European League Against Rheumatism collaborative initiative. *Arthritis Rheum* **62**, 2569-2581 (2010).
62. R. Altman, E. Asch, D. Bloch, G. Bole, D. Borenstein, K. Brandt, W. Christy, T. D. Cooke, R. Greenwald, M. Hochberg, et al., Development of criteria for the classification and reporting of osteoarthritis. Classification of osteoarthritis of the knee. Diagnostic and Therapeutic Criteria Committee of the American Rheumatism Association. *Arthritis and rheumatism* **29**, 1039-1049 (1986).
63. M. Armaka, V. Gkretsi, D. Kontoyiannis, G. Kollias, A standardized protocol for the isolation and culture of normal and arthritogenic murine synovial fibroblasts. (2009).
64. T. Stuart, A. Butler, P. Hoffman, C. Hafemeister, E. Papalexi, W. M. Mauck, 3rd, Y. Hao, M. Stoeckius, P. Smibert, R. Satija, Comprehensive Integration of Single-Cell Data. *Cell* **177**, 1888-1902 e1821 (2019).
65. Z. Xie, A. Bailey, M. V. Kuleshov, D. J. B. Clarke, J. E. Evangelista, S. L. Jenkins, A. Lachmann, M. L. Wojciechowicz, E. Kropiwnicki, K. M. Jagodnik, M. Jeon, A. Ma'ayan, Gene Set Knowledge Discovery with Enrichr. *Current protocols* **1**, e90 (2021).
66. S. Alivernini, L. MacDonald, A. Elmesmari, S. Finlay, B. Tolusso, M. R. Gigante, L. Petricca, C. Di Mario, L. Bui, S. Perniola, M. Attar, M. Gessi, A. L. Fedele, S. Chilaka, D. Somma, S. N. Sansom, A. Filer, C. McSharry, N. L. Millar, K. Kirschner, A. Nerviani, M. J. Lewis, C. Pitzalis, A. R. Clark, G. Ferraccioli, I. Udalova, C. D. Buckley, E. Gremese, I. B. McInnes, T. D. Otto, M. Kurowska-Stolarska, Distinct synovial tissue macrophage subsets regulate inflammation and remission in rheumatoid arthritis. *Nat Med* **26**, 1295-1306 (2020).

67. I. Korsunsky, N. Millard, J. Fan, K. Slowikowski, F. Zhang, K. Wei, Y. Baglaenko, M. Brenner, P. R. Loh, S. Raychaudhuri, Fast, sensitive and accurate integration of single-cell data with Harmony. *Nat Methods* **16**, 1289-1296 (2019).
68. T. D. Schmittgen, K. J. Livak, Analyzing real-time PCR data by the comparative C(T) method. *Nat Protoc* **3**, 1101-1108 (2008).
69. V. Haberle, A. R. Forrest, Y. Hayashizaki, P. Carninci, B. Lenhard, CAGEr: precise TSS data retrieval and high-resolution promoterome mining for integrative analyses. *Nucleic Acids Res* **43**, e51 (2015).
70. M. Thodberg, A. Thieffry, K. Vitting-Seerup, R. Andersson, A. Sandelin, CAGEfightR: analysis of 5'-end data using R/Bioconductor. *BMC Bioinformatics* **20**, 487 (2019).
71. H. Li, R. Durbin, Fast and accurate short read alignment with Burrows-Wheeler transform. *Bioinformatics* **25**, 1754-1760 (2009).
72. E. P. Consortium, An integrated encyclopedia of DNA elements in the human genome. *Nature* **489**, 57-74 (2012).
73. M. M. Hoffman, J. Ernst, S. P. Wilder, A. Kundaje, R. S. Harris, M. Libbrecht, B. Giardine, P. M. Ellenbogen, J. A. Bilmes, E. Birney, R. C. Hardison, I. Dunham, M. Kellis, W. S. Noble, Integrative annotation of chromatin elements from ENCODE data. *Nucleic Acids Res* **41**, 827-841 (2013).
74. H. Li, B. Handsaker, A. Wysoker, T. Fennell, J. Ruan, N. Homer, G. Marth, G. Abecasis, R. Durbin, S. Genome Project Data Processing, The Sequence Alignment/Map format and SAMtools. *Bioinformatics* **25**, 2078-2079 (2009).
75. A. Dobin, C. A. Davis, F. Schlesinger, J. Drenkow, C. Zaleski, S. Jha, P. Batut, M. Chaisson, T. R. Gingeras, STAR: ultrafast universal RNA-seq aligner. *Bioinformatics* **29**, 15-21 (2013).
76. Y. Liao, G. K. Smyth, W. Shi, The Subread aligner: fast, accurate and scalable read mapping by seed-and-vote. *Nucleic acids research* **41**, e108 (2013).
77. M. I. Love, W. Huber, S. Anders, Moderated estimation of fold change and dispersion for RNA-seq data with DESeq2. *Genome Biol* **15**, 550 (2014).
78. H. P. Kiener, G. F. Watts, Y. Cui, J. Wright, T. S. Thornhill, M. Sköld, S. M. Behar, B. Niederreiter, J. Lu, M. Cernadas, A. J. Coyle, G. P. Sims, J. Smolen, M. L. Warman, M. B. Brenner, D. M. Lee, Synovial fibroblasts self-direct multicellular lining architecture and synthetic function in three-dimensional organ culture. *Arthritis Rheum* **62**, 742-752 (2010).
79. M. T. Veeman, D. C. Slusarski, A. Kaykas, S. H. Louie, R. T. Moon, Zebrafish prickle, a modulator of noncanonical Wnt/Fz signaling, regulates gastrulation movements. *Current biology : CB* **13**, 680-685 (2003).
80. J. E. Jonkman, J. A. Cathcart, F. Xu, M. E. Bartolini, J. E. Amon, K. M. Stevens, P. Colarusso, An introduction to the wound healing assay using live-cell microscopy. *Cell adhesion & migration* **8**, 440-451 (2014).

Supplementary Files

This is a list of supplementary files associated with this preprint. Click to download.

- Suppl.FiguresHOTAIR20221107v20.pdf
- SupplementaryTables20221222ME.pdf
- Movie.mp4